

# 博士論文(要約)

## **Development of novel fluorescent probes based on rhodol scaffolds for live cell/tissue imaging**

(新規ロドール型蛍光プローブの開発と細胞・組織の  
ライブ蛍光可視化への応用)

鹿 島 大 幹

**Development of novel fluorescent probes based on  
rhodol scaffolds for live cell/tissue imaging**

(新規ロドール型蛍光プローブの開発と細胞・組織の  
ライブ蛍光可視化への応用)

東京大学 大学院医学系研究科

生体物理医学専攻 医用生体工学講座

生体情報学分野

指導教員 浦野 泰照 教授

申請者 鹿島 大幹

# **Contents**

## **Abstract**

## **1. Introduction**

- 1.1 Molecular imaging
- 1.2 Conventional fluorescent probes
- 1.3 Fluorescence control mechanism for activatable fluorescent probes

## **2. Photoactivatable fluorophores for durable labeling of individual cells**

- 2.1 Photoactivatable fluorophores
- 2.2 SPiDER probes
- 2.3 Purpose of research
- 2.4 Development of paSPiDERs
- 2.5 Evaluation of probes *in vitro*
  - 2.5.1 Optical properties of paSPiDERs
  - 2.5.2 Photoactivation

2.5.3 Tracing of photo-reaction with LC-MS

2.5.4 Protein labeling

## 2.6 Evaluation of probes *in cellulo*

2.6.1 Fluorescent cell labeling by photoirradiation and resistance to fixation

2.6.2 Single cell labeling by photoirradiation

2.6.3 Long time imaging

2.6.4 Dark toxicity and phototoxicity

## 2.7 Tissue imaging *ex vivo*

## 2.8 Brief summary

# **3. Activatable Orange fluorescent probes based on carborhodol scaffold**

## 3.1 Cancer imaging

## 3.2 Purpose of research

## 3.3 Development of new orange fluorophores based on carborhodol scaffold

### 3.3.1 Synthesis of basic CR scaffolds

### 3.3.2 CR derivatives with a hydroxyalkyl group

3.3.2 CR derivatives with a carboxy group

3.3.3 Prediction of  $pK_{\text{cycl}}$  values by computational chemistry

### 3.4 Activatable orange fluorescent probes for $\beta$ -galactosidase

3.4.1 Synthesis of probes

3.4.2 Optical properties

3.4.3 Enzyme reaction

3.4.4 Reaction tracking with LCMS

3.4.5 Live-cell imaging of  $\beta$ -galactosidase activity

### 3.5 Brief summary

## 4. Conclusion

4.1 Overview

4.2 Discussion and future prospect

## 5. Experimental section

## References

## Acknowledge

## Abstract

Fluorescence imaging in combination with fluorescent probes has been widely used to visualize specific biological phenomena and to understand physico-pathological conditions in real time. In this study, I designed and developed two types of novel fluorescent probes. First one is photoactivatable fluorophores with improved intracellular retention, and second one is a new activatable orange-emitting fluorescence probe for  $\beta$ -galactosidase based on carborhodol scaffolds.

Photoactivatable fluorophores are photofunctional small molecules that are weakly fluorescent before light irradiation but recover their original fluorescence after light irradiation. However, most of the existing photoactivatable fluorophores lack of sufficient cell membrane permeability and intracellular retention. In this study, I have designed and developed non-fluorescent, cell-permeable photoactivatable fluorophores, photoactivatable SPiDERs (paSPiDERs), exhibiting fluorescence activation upon light irradiation, accompanied by the generation of a quinone methide intermediate that binds covalently to intracellular proteins. The fluorescence signal is durable for 24 hours, resistant to fixation and compatible with immunostaining, and selective cell labeling can

be achieved at single-cell resolution.

Activatable fluorescent probes targeting enzymes upregulated in cancer have been developed for specific cancer imaging. Here, I developed orange-emitting fluorescent probes that can potentially be used in combination with green and red fluorescent probes in order to detect cancer sites with improved sensitivity and specificity. By means of a synthetic approach to finding a suitable scaffold dye for activatable probe of our purpose, I developed new series of orange-emitting carborhodol dyes and found a promising scaffold. Based on the scaffold, I developed a highly activatable fluorescence probe for  $\beta$ -galactosidase and successfully achieved fluorescence imaging of the enzyme-expressing cells.

# **Chapter 1**

## **Introduction**



## 1.1 Molecular imaging

The elucidation of biological phenomena is the primary aim of life science. Since living organisms are composed of a wide variety of cells, and their properties change depending on the surrounding conditions, *in vivo* visualization is indispensable for their analysis. In the field of medicine, technology to visualize biological functions related to diseases can be also powerful diagnostic tools.

Molecular imaging modalities, which visualize activity levels, localizations of tissues and biomolecules in real-time, have attracted strong attention from medical fields over recent years. Magnetic resonance imaging (MRI), X-ray computed tomography (X-ray CT), ultrasonography (ultrasound), positron emission tomography (PET), and single photon emission computed tomography (SPECT) have become indispensable modalities to detect diseases, and to make a decision in guide treatments.

**Table 1.1** Properties of cancer imaging modalities.

Technique	Resolution		Depth <sup>c</sup>	Multi-channel	Cost <sup>d</sup>	Imaging agent	
	Space <sup>a</sup>	Time <sup>b</sup>				Example	Activat-ability <sup>e</sup>
MRI	⊙	△	⊙	×	\$\$\$	Paramagnetic chelates etc.	○
CT	⊙	○	⊙	×	\$\$	Iodinated molecules	×
Ultrasound	⊙	○	○	×	\$\$	Microbubbles	×
PET	○	△	⊙	×	\$\$\$	<sup>18</sup> F-labelled compounds etc.	×
SPECT	○	△	⊙	×	\$\$	<sup>99m</sup> Tc-labelled compounds etc.	×
Fluorescence	⊙	⊙	△	○	\$	Fluorochromes, photoproteins	⊙

Adapted mainly from Weissleder *et al.*<sup>1</sup> <sup>a</sup>⊙, < 1 mm; ○, 1–2 mm. <sup>b</sup>⊙, msec; ○, sec–min; △, min–hr. <sup>c</sup>Tissue penetration; ⊙, no limit; ○, cm; △, < 1 cm. <sup>d</sup>Cost is based on purchase price of the imaging system in the United States: \$, < US\$ 101,000; \$\$, US\$ 101,000–300,000; \$\$\$, > US\$ 300,000. <sup>e</sup>Activation rate of imaging signal [fold] ; ⊙, no limit; ○, ~10; ×, 1.

While various modalities have been developed, fluorescence imaging, which mainly utilizes visible light, is a representative method for detecting biomolecules and biological phenomena. Due to its high sensitivity, spatiotemporal resolution and Tumor to Non-tumor (T/N) ratio, fluorescence imaging techniques have been applied to various biological experiments and clinical diagnoses.

## 1.2 Conventional fluorescent probes for live cell imaging

Fluorescence imaging is a research technique to visualize dynamics of biomolecules in living cells and tissues. By using functional molecules called “fluorescent probes” that specifically emit fluorescence signals in the presence of particular biomolecules or biological phenomena, we can visualize the target information in real time.

Fluorescent probes mainly belong to three types: small organic molecules, biomolecules such as fluorescent proteins, and semiconductor particles such as quantum dots. Among them, small organic molecules are widely used in the life science and medical fields especially due to their relatively high brightness and high photo-resistance properties. In addition, their chemical and optical properties can be designed depending on the biological target by synthetic approaches.

Before the late of 19<sup>th</sup> century, small fluorescent molecules had not been caught an attention in biological applications due to its excitation wavelength in the UV range. However, the development of green-emitting fluorophore, fluorescein reported by Baeyer *et al.* at the end of the 19th century changed this situation<sup>2</sup>. The development of fluorescein isothianate (FITC) reported by Coon *et al.* in 1942 also attracted a great deal of attention as small-molecular dyes that can be excited by the UV visible light<sup>3</sup>. These

findings brought the direction of small-molecular dyes for biological imaging using fluorescence microscopy. Research on fluorescent dyes has continued until today, and the various fluorescent molecules have been developed: dipyrromethene (BODIPY)<sup>4</sup>, known for its high brightness; Rhodamine, used in DNA sequencing<sup>5, 6</sup>; CyDye, Alexa Fluoro, ATTO series, developed as an improved version of Rhodamine and other fluorescent dyes<sup>7, 8</sup>. The research on fluorescent dyes continued unabated for decades, including the application of new chemistry to small-molecule dye synthesis, the advent of super-resolution microscopy and single molecule microscopy, and the creation of new labeling strategies such as small molecule-protein hybrid systems<sup>9, 10</sup>, which is useful in living cells and tissues<sup>11-13</sup>.

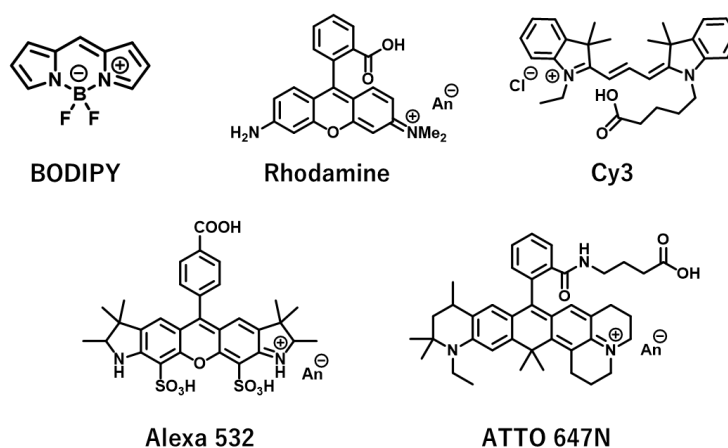


**Fig. 1.1** The existing small-molecular fluorescent dyes and their structures

### **1.3 Fluorescence control mechanism for activatable fluorescent probes**

While various bioimaging methods have been developed with fluorescent dyes, most of them are "always-on" fluorescent probes emitting constant fluorescence. They can potentially cause non-specific fluorescent signals by labeling to non-target biomolecules or by showing non-target distribution (Fig. 1.2, above).

On the other hands various “activatable” type fluorescent probes that are initially non-fluorescent before reaction with target molecules, but emit fluorescence signals in the presence of the target molecules has been developed. By using activatable fluorescence probe, the background signals can be suppressed compared to that of always-on type fluorescent probes, enabling us to visualize target molecules specifically. In the case of cancer imaging with activatable probes, the background signals at non-lesion sites are suppressed to achieve higher T/N ratio, compared to always-on type probes (**Fig. 1.2**, bottom).

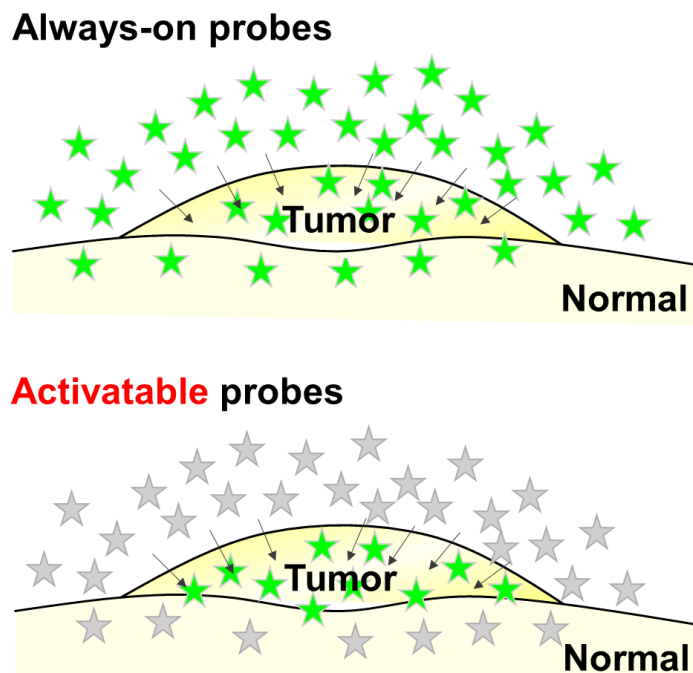


**Fig. 1.2** Always-on type fluorescent probe and activatable type fluorescent probe.

There are several mechanisms for controlling fluorescence signals; 1) Photoinduced electron Transfer (PeT), 2) Internal charge transfer (ICT), 3) Intramolecular spirocyclization (Formation/cleavage of  $\pi$ -conjugation) and 4) Förster resonance energy transfer (FRET), etc. It is an important to select appropriate mechanism to design fluorescent probes with the desired functions.

Our laboratory previously reported a highly sensitive activatable fluorescent probe for  $\gamma$ -glutamyltranspeptidase (GGT), gGlu-HMRG, which can specifically detect cancer cells with GGT expression<sup>14</sup>. The fluorescence of this probe was precisely controlled by the

mechanism of intramolecular spirocyclization (mechanism of **3**). As GGT has been known to be up-regulated in several cancer, this probe has realized rapid and highly sensitive detection of cancer tissues in clinical specimens that cannot be identified by naked eyes.

gGlu-HMRG is based on hydroxymethyl rhodamine (HMR), which is a group of rhodamines possessing a nucleophilic hydroxymethyl group (HM group) at 2-position of the benzene ring of rhodamines. HMRs show the chemical equilibrium of intramolecular spirocyclization by nucleophilic attack of the HM group on the electron-deficient 9<sup>th</sup> carbon atom of xanthene ring, and exist as an equilibrium between open and closed forms in protic solvents. The open form shows strong fluorescence derived from the xanthene ring while the closed form takes a non-fluorescent spirocyclic structure in which the p-conjugation system is cleaved. By precisely controlling the intramolecular spirocyclization behavior of HMRs, various activatable fluorescent probes for cancer-associated enzymatic activities have successfully developed in our laboratory<sup>15-18</sup>. In the case of water-containing solvents, the equilibrium between the open and closed forms of HMRs changes reversibly depending on the pH of the solvent, and this ratio can be measured by the intensity of absorption and fluorescence derived from the xanthene ring. The  $pK_{cycl}$  is defined as the pH value at which the extent of spirocyclization is sufficient

to reduce the absorbance of the compound to one-half of the maximum absorbance. Recently, Tachibana *et. al.* showed that  $pK_{\text{cycl}}$  is strongly affected not only by the chemical structure, but also by the measured solvation<sup>19</sup>. In particular, the  $pK_{\text{cycl}}$  can be predicted relatively accurately by considering the cross-linking pattern between water molecules and the compound under aqueous solvents.

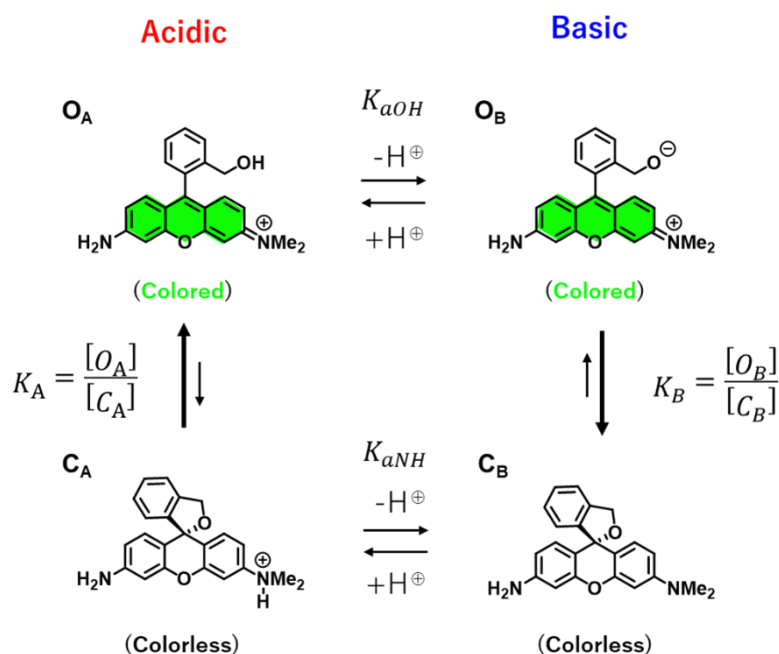


**Fig. 1.3** Equilibrium state between closed form and open form of HMRG.

The fluorescence control by intramolecular spirocyclization has been used to design novel fluorescent probes developed in **Chapters 2** and **3** of this doctoral thesis.



## **Chapter 2**

Photoactivatable fluorophores for durable labelling  
of individual cells

## 2.1 Photoactivatable fluorophores

Small-molecular photoactivatable fluorophores (PAFs, caged fluorophores) are fluorophores whose fluorescence is initially suppressed, but can be photochemically converted to fluorescent molecules upon light irradiation<sup>20,21</sup> (**Fig. 2.1.1**).

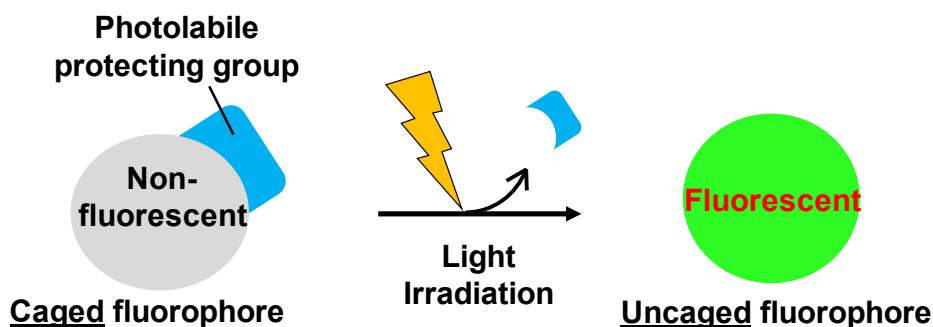


**Fig. 2.1.1** The photoactivation scheme of PAFs.

Various kinds of PAFs have been developed and they have proved to be powerful imaging tools for super-resolution imaging<sup>22-24</sup>, and for tracking molecular and cellular dynamics with high spatiotemporal resolution.<sup>23-27</sup> For example, PAFs with intracellular esterase-reactive groups such as acetoxymethyl (AM) can also be retained in cells upon hydrolysis of the reactive group, but leakage of the fluorescent hydrolysis product from the cells during prolonged observation and/or

fixation can be a problem<sup>25, 28</sup> (**Fig. 2.1.2**). In contrast, small-molecular PAFs with thiol-reactive groups such as iodoacetamide (IAA) are cell-membrane permeable, but can be retained in cells due to the formation of adducts with intracellular nucleophiles such as proteins<sup>21</sup>. However, the promiscuous labelling of both target and non-target cells can potentially cause cytotoxicity in the absence of light irradiation (i.e., dark toxicity) due to the consumption of essential thiol-containing molecules in the cells. Combination with self-labelling proteins may solve these problems, but require genetic manipulation<sup>29, 30</sup>. PAFs conjugated to dextran polymers had been used for selective cell labeling for long-term cell tracking or for cell-cell junctional coupling in vivo without genetic manipulations. However, these conjugates need to be injected into cells<sup>31-33</sup>.

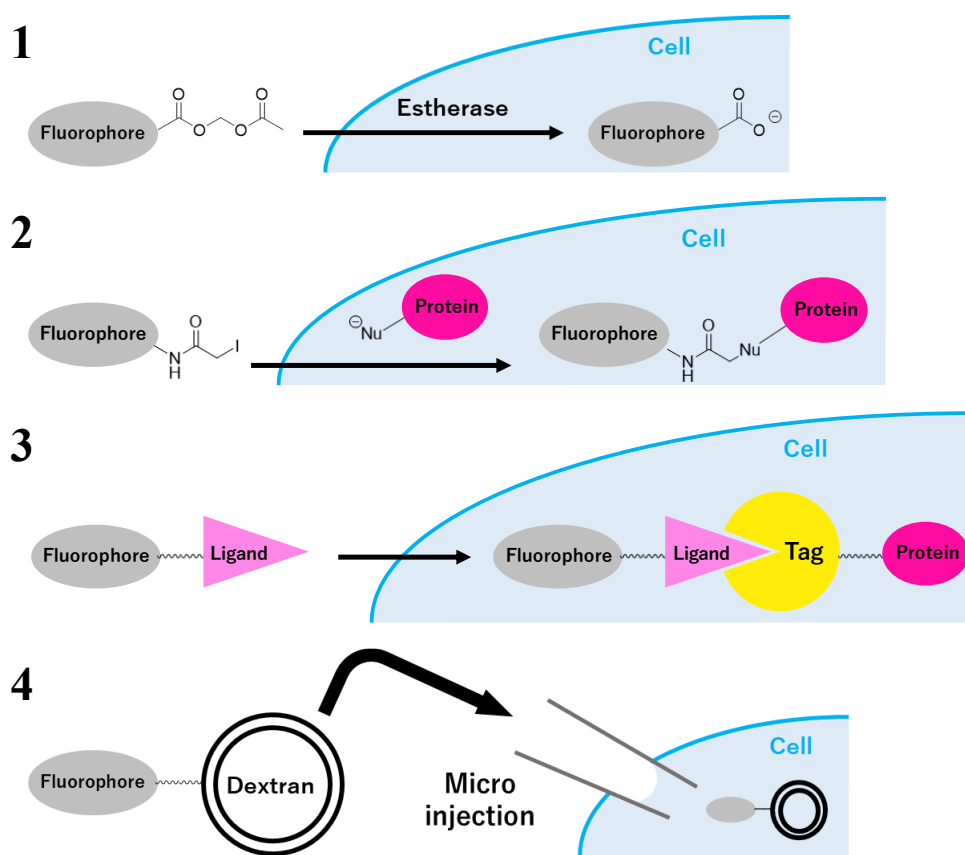


**Fig. 2.1.2** Representative mechanism for being retained in living cells. 1) AM group, 2) IAA group, 3) tag-proteins, 4) micro injection

Although some recently reported fluorogenic photoaffinity labelling (PAL) probes enable fluorogenic labelling of specific protein without dark toxicity<sup>34, 35</sup>, these PAL probes require relatively short-wavelength excitation for fluorescence imaging. Therefore, to achieve specific cell labelling and imaging with longer wavelength, there is still a need for cell-permeable PAFs that do not influence cell functions in the dark, but exhibit both fluorescence activation and acquisition of anchoring ability to intracellular proteins in response to light irradiation.

## 2.2 SPiDER probes

In this report, I describe new small-molecular PAFs that meet these requirements.

To develop suitable molecules, I focused on our previously reported fluorescent probes for  $\beta$ -galactosidase (SPiDER- $\beta$ Gals)<sup>36</sup> and  $\gamma$ -glutamyltranspeptidase (4-CH<sub>2</sub>F-HMDiEtR-gGlu)<sup>37</sup>, which were designed so that reaction with the enzymes would produce electrophilic (aza)quinone methide intermediates that could be trapped by intracellular nucleophiles (Fig. 2.2.1).

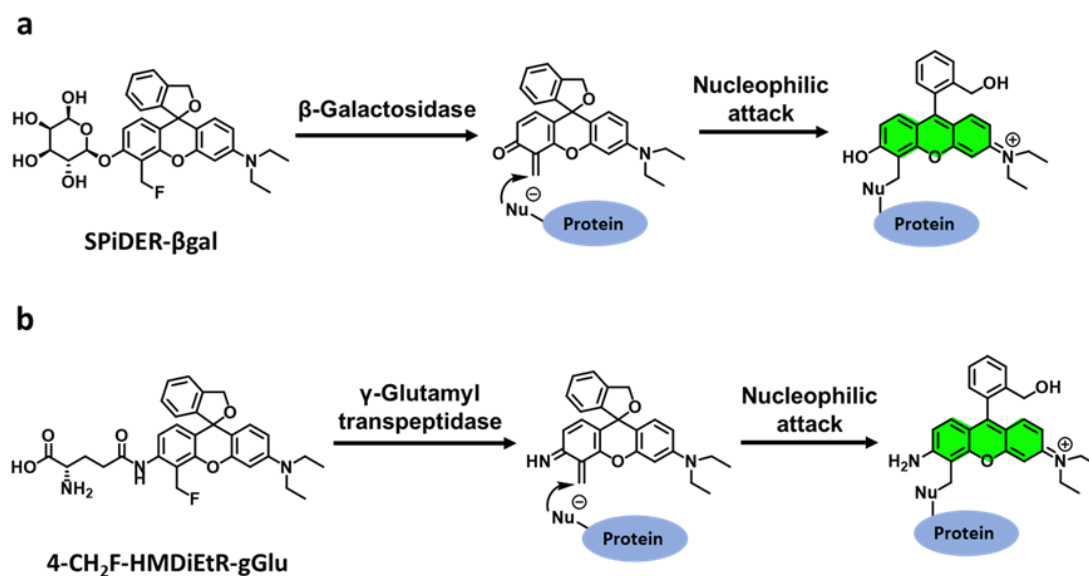


**Fig. 2.2.1** The reaction scheme of SPiDER- $\beta$ Gal (a) and 4-CH<sub>2</sub>F-HMDiEtR-gGlu (b)

These probes are designed to react with the target enzymes to simultaneously acquire fluorescence and intracellular retention by combining "fluorescence control based on intramolecular spirocyclization" and "intracellular retention control based on quinone methide chemistry".

Quinone methide chemistry is a chemistry that has been applied to develop enzyme inhibitors<sup>38</sup>, activity-based probes<sup>39</sup>, self-immolative fluorescent probes<sup>40, 41</sup>, and prodrugs<sup>42</sup>. For example, when a leaving group such as a fluoromethyl group is present at the ortho- or para-position of a phenyl ether, the cleavage of the ether bond to form a phenolic hydroxyl group leads to the release of the leaving group, producing a quinone methide intermediate, which is rapidly trapped by the surrounding nucleophile molecules (**Fig. 2.2.2**).



**Fig. 2.2.2** Generation of and nucleophilic addition to a quinone methide. Adapted mainly from D. H. Kwan *et al.*<sup>41</sup>.

For example, SPiDER- $\beta$ Gal is colourless and nonfluorescent at physiological pH because it exists as the closed spirocyclic structure. However, upon hydrolysis by

intracellular  $\beta$ -galactosidase, the fluorine atom is released to generate an electrophilic quinone methide intermediate, which then reacts with intracellular nucleophilic molecules such as proteins to be fluorescent. The fluorescent dye labelled to the intracellular protein does not leak out of the cell, thus preventing diffusion of the fluorescent dye to be retained in cells. As a result, *lacZ*-expressing cells (cells expressing the reporter enzyme  $\beta$ -galactosidase from *E. coli*) in living tissues can be successfully visualized at the single-cell resolution (**Fig. 2.2.3**).

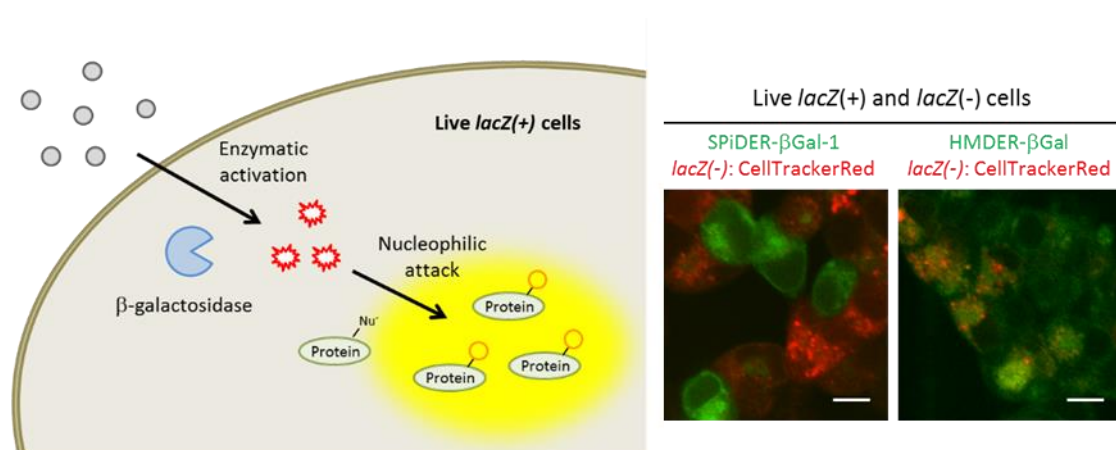


**Fig. 2.2.3** Functionalized fluorogenic substrates for  $\beta$ -galactosidase in living *lacZ*(+) cells (SPiDER-βGals). Reprinted with permission from reference<sup>36</sup>.

## 2.3 Purpose of this research

In this study, I attempt to develop a new photoactivatable fluorophore that can be used easily and without genetic manipulations in samples with a mixture of various cells or tissues, by following the molecular design of SPiDER- $\beta$ Gal to simultaneously activate fluorescence and intracellular retention upon light irradiation. I developed a photoactivatable fluorophore, photoactivatable SPiDER (paSPiDER), which is nonfluorescent and cell-permeable before light irradiation, but produce an active intermediate quinone methide upon light irradiation, which is then attacked by intracellular nucleophiles (proteins, GSH, etc.) and then stays inside the cell (Fig. 2.3.1).

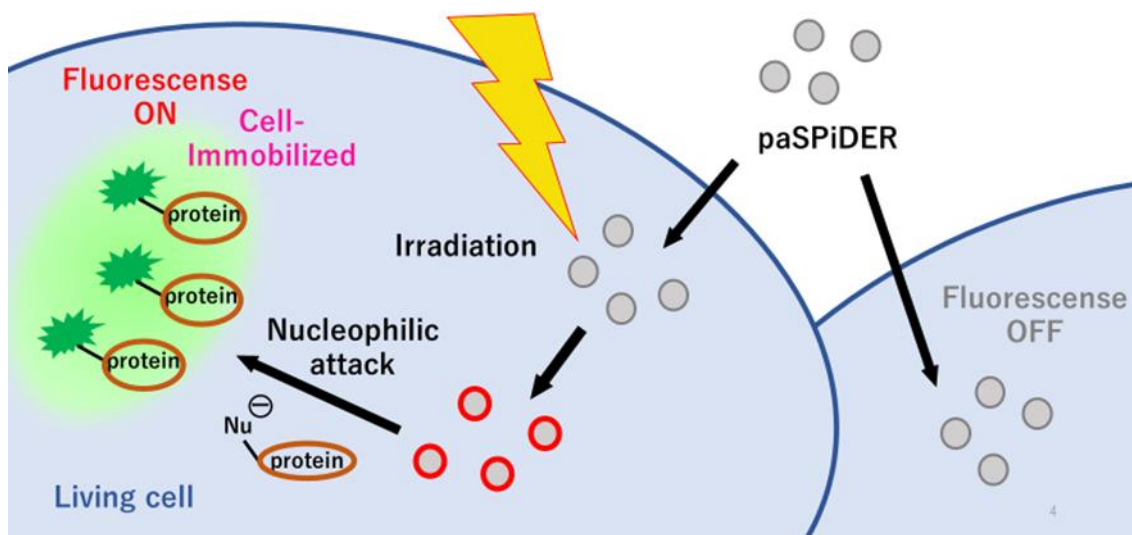


**Fig. 2.3.1** Activation mechanism of paSPiDERs; activation of fluorescence and binding ability to intracellular proteins occur by photo-irradiation so that the fluorescent product is immobilized in living cells.



## 2.4 Development of paSPiDERs

Based on the molecular design of SPiDER- $\beta$ Gal, I prepared rhodol-based photoactivatable SPiDER-1 (paSPiDER-1) and rhodamine-based paSPiDER-2 by replacing the  $\beta$ -galactosyl moiety of SPiDER- $\beta$ Gal and the  $\beta$ -glutamyl moiety of 4-CH<sub>2</sub>F-HMDiEtR-gGlu with a photolytic protecting group, the 4,5-dimethoxy nitrobenzyl group (DMNB) (**Fig. 2.4.1, Scheme 2.4.1**)<sup>43</sup>. I selected DMNB as a caging group because of its relatively long absorbance<sup>44, 45</sup>, so that uncaging could be achieved with a commonly used 405 nm laser. The resulting PAFs were expected to be initially non-fluorescent and cell-permeable, but to exhibit durable fluorescence activation in light-irradiated target cells via covalent binding to intracellular proteins.

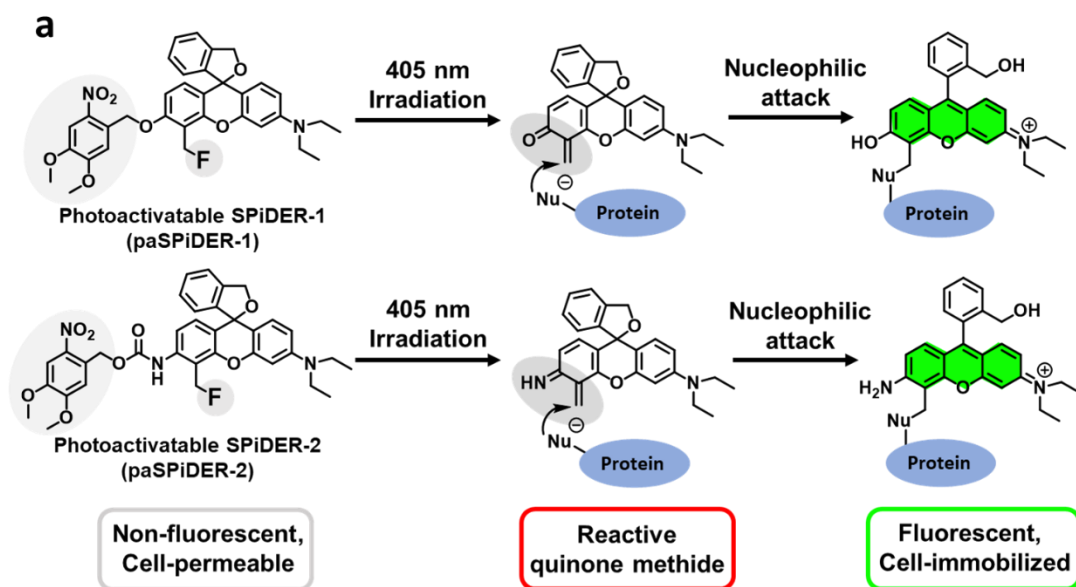
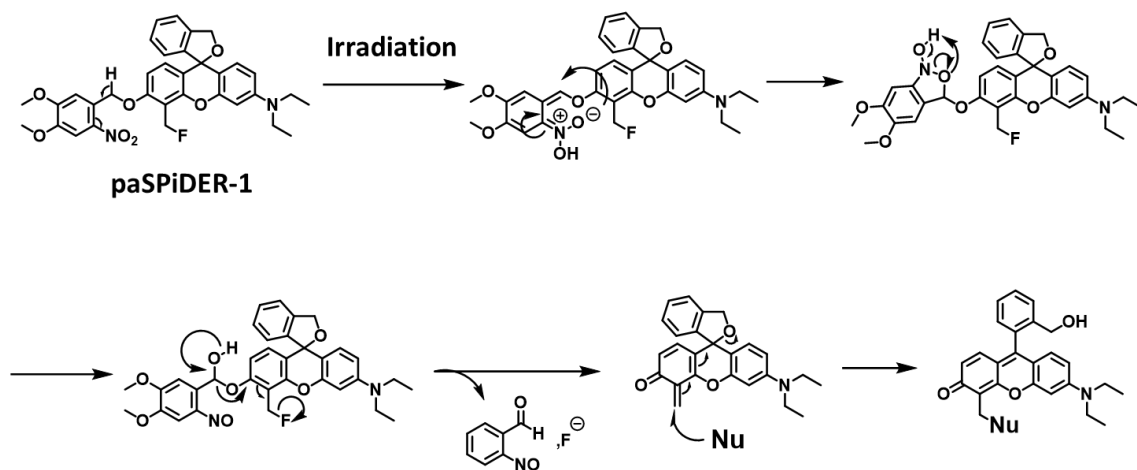


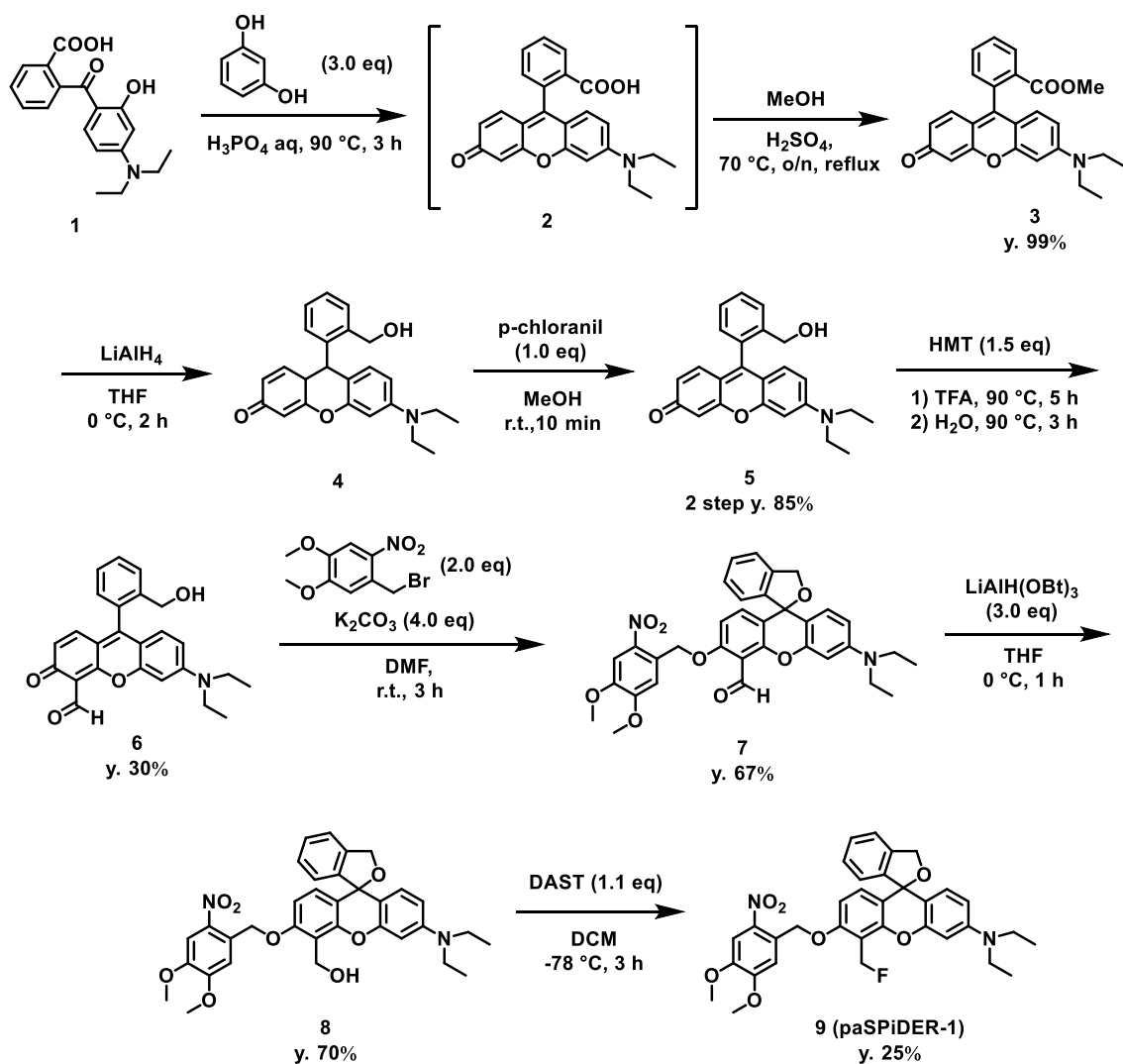
**Fig. 2.4.1 (a)** Molecular design of **paSPiDER-1** (upper) and **paSPiDER-2** (bottom), and the activation mechanism of fluorescence and binding ability to intracellular nucleophiles, such as proteins, by photo-irradiation so that the fluorescent products are immobilized in living cells.



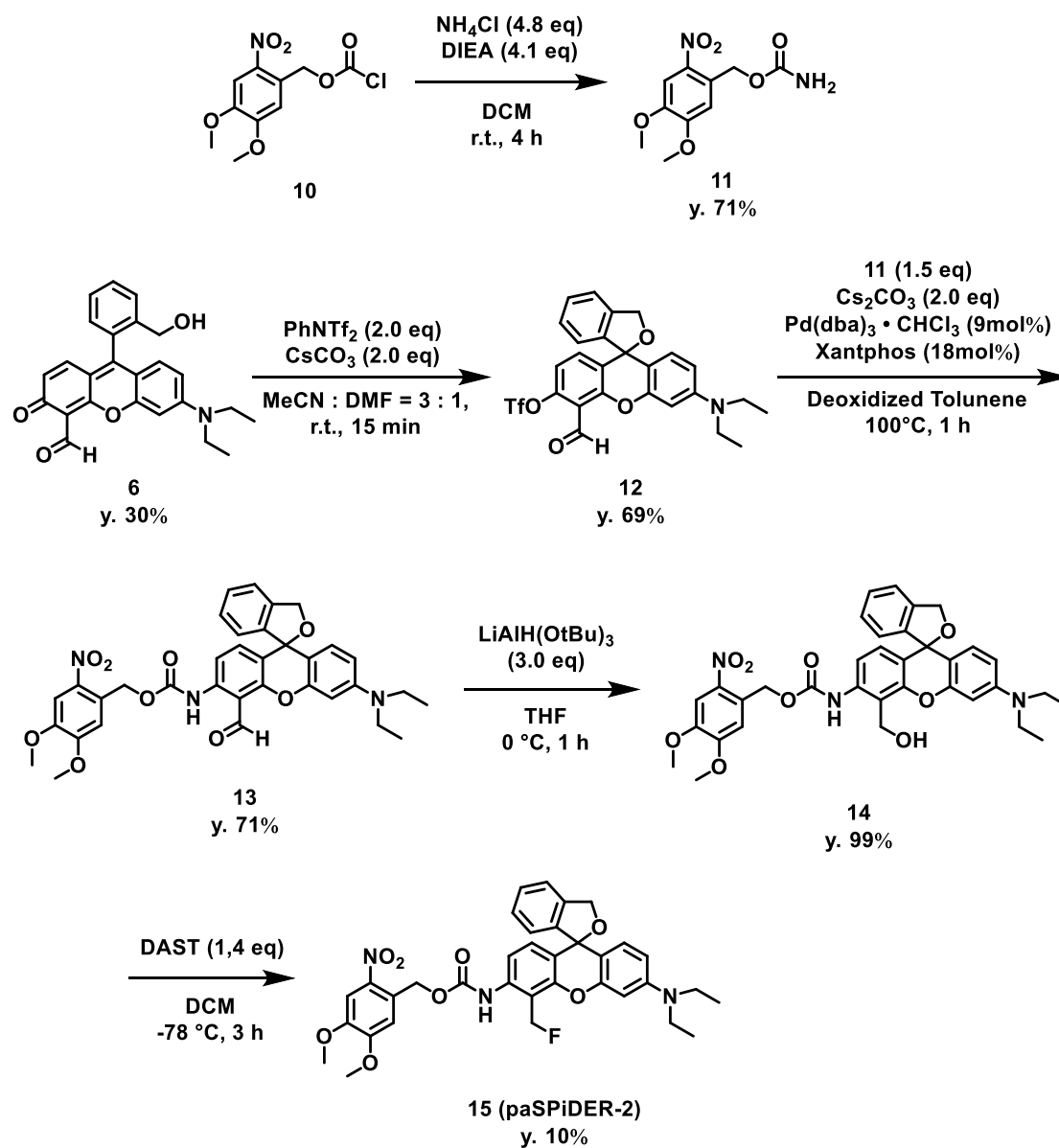
**Scheme 2.4.1.** Reaction scheme of paSPiDER-1 in response to light irradiation, showing the activation mechanism of fluorescence and covalent binding to intracellular nucleophiles.

paSPiDERs are synthesized as follows with reference to the previous reports<sup>36</sup>.

37



Scheme 2.4.2. Synthetic scheme of paSPiDER-1.



**Scheme 2.4.3.** Synthetic scheme of paSPiDER-2.

## 2.5 Evaluation of probes *in vitro*

### 2.5.1 Optical properties

To validate our design strategy, I first evaluated the optical properties of paSPiDERs in aqueous solution. As expected, the absorbance and fluorescence spectra at various pHs showed that paSPiDERs exhibited a pH-dependent equilibrium of intramolecular spirocyclization; they exist in the colored xanthene form with absorption and emission in the visible wavelength range at acidic pH, whereas they exist in the colorless spirocyclic form at neutral and alkaline pHs. The values of  $pK_{cycl}$  (the pH at which the extent of spirocyclization is sufficient to reduce the absorbance of the compound to one-half of the maximum absorbance)<sup>46</sup> of paSPiDER-1 and paSPiDER-2 were calculated to be 3.4 and 3.5, respectively, indicating that these paSPiDERs mainly exist in the colorless and non-fluorescent form at the physiological pH of 7.4 (**Fig. 2.5.1, 2.5.2, Table 2.5.1**). The fluorescence quantum yields ( $\Phi_f$ ) of the open forms of paSPiDER-1 and paSPiDER-2 were also suppressed to 0.01, suggesting that the background fluorescence signal would be low. In contrast, the  $pK_{cycl}$  values of 4-CH<sub>2</sub>OH-HMDER and 4-CH<sub>2</sub>OH-HMDiEtR, the model reaction products of paSPiDER-1 and paSPiDER-2, were reported to be 11.4 and 9.6, respectively, indicating that they would mainly exist as the colored, fluorescent open

forms at pH 7.4 ( $\Phi_{\text{fl}} = 0.11$  for 4-CH<sub>2</sub>OH-HMDER and 0.04 for 4-CH<sub>2</sub>OH-HMDiEtR).

Taken together, these results indicate that the paSPiDERs function as highly fluorogenic PAFs.

The following table summarizes the optical properties of paSPiDER-1, paSPiDER-2, 4-CH<sub>2</sub>OH-HMDER and 4-CH<sub>2</sub>OH-HMDiEtR, which are formed by the addition of water molecules to the quinone methide intermediate produced after photoirradiation (**Table 2.5.1**).

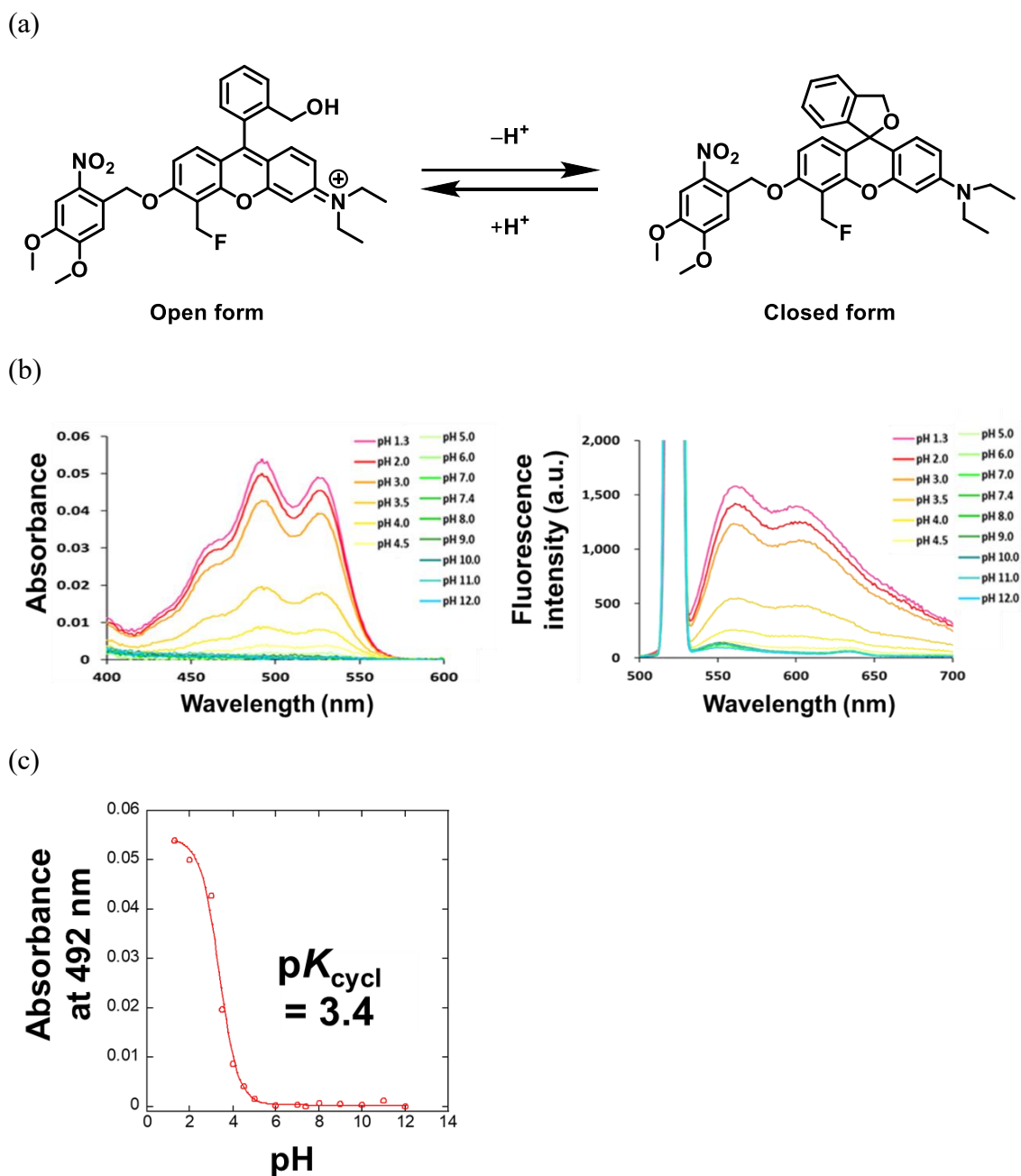


**Fig. 2.5.1-1** pH dependency of absorption and fluorescence spectra. (a) Acid-base equilibrium and pH-dependent spirocyclization of **paSPiDER-1**. (b) pH dependent absorption (left) and fluorescence (right) spectra. Absorption and fluorescence spectra of 1  $\mu$ M paSPiDER-1 at various pH values in 0.2 M sodium phosphate buffer, containing, 1% DMSO as a cosolvent. (c) Maximum absorbance at 492 nm was plotted against pH.

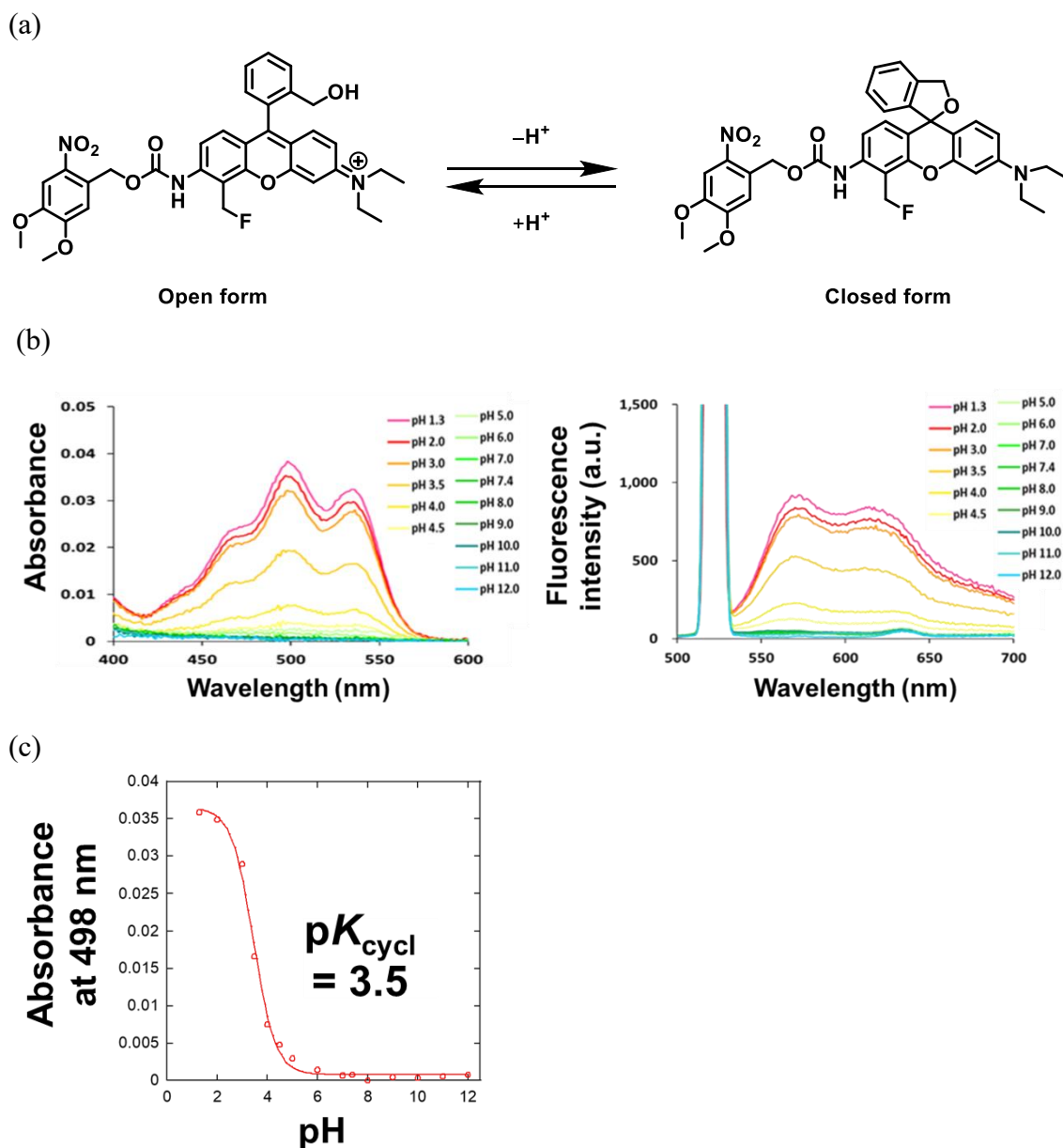


**Fig. 2.5.1-2** pH dependency of absorption and fluorescence spectra. (a) Acid-base equilibrium and pH-dependent spirocyclization of **paSPiDER-2**. (b) pH dependent absorption (left) and fluorescence (right) spectra. Absorption and fluorescence spectra of 1  $\mu$ M paSPiDER-2 at various pH values in 0.2 M sodium phosphate buffer, containing 0.1% DMSO as a cosolvent. (c) Maximum absorbance at 498 nm was plotted against pH.



**Table 2.5.1.** Photophysical properties of paSPiDERs and the putative photo-reaction products <sup>a)</sup>

	Abs <sub>max</sub> (nm)	Em <sub>max</sub> (nm)	$\epsilon$ (M <sup>-1</sup> cm <sup>-1</sup> )	$\Phi_{\text{fl}}$	p <i>K</i> <sub>cycl</sub>	Brightness ( $\epsilon \times \Phi_{\text{fl}}$ )
<b>paSPiDER-1</b>	493, 527 <sup>b)</sup>	561, 601 <sup>b)</sup>	52,000 <sup>b)</sup>	0.01 <sup>b)</sup>	3.4	520
<b>paSPiDER-2</b>	498, 533 <sup>b)</sup>	570, 620 <sup>b)</sup>	38,000 <sup>b)</sup>	0.01 <sup>b)</sup>	3.5	380
<b>4-CH<sub>2</sub>OH-HMDER</b>	526 <sup>c)</sup>	553 <sup>c)</sup>	120,000 <sup>b)</sup>	0.11 <sup>c)</sup>	11.4 <sup>c)</sup>	13,200
<b>4-CH<sub>2</sub>OH-HMDiEtR</b>	534 <sup>d)</sup>	558 <sup>d)</sup>	100,000 <sup>b)</sup>	0.04 <sup>d)</sup>	9.6 <sup>d)</sup>	4,000

<sup>a)</sup>Absorption maximum ( $\lambda_{\text{abs}}$ ), fluorescence emission maximum ( $\lambda_{\text{em}}$ ), molar extinction coefficient ( $\epsilon$ ), fluorescence quantum yield ( $\Phi_{\text{fl}}$ ), equilibrium constant for intramolecular spirocyclization (p*K*<sub>cycl</sub>), relative brightness ( $\epsilon \times \Phi_{\text{fl}}$ ). <sup>b)</sup>Measured in 200 mM sodium phosphate buffer (pH 2.0). <sup>c)</sup>Reference 14. <sup>d)</sup>Reference 15.

### 2.5.2 Photoactivation test

I next examined the photoactivation properties of the paSPiDERs. When solutions of the paSPiDERs in 200 mM sodium phosphate buffer at pH 7.4 were illuminated with 405 nm light from a xenon source, I observed significant increases of absorption and fluorescence intensity in the visible region in a time-dependent manner, suggesting that the paSPiDERs were converted to the colored and fluorescent hydrolysis products (**Fig. 2.5.2**). However, especially in the case of paSPiDER-2, I noticed that the absorption maximum shifted to shorter wavelength, depending on the irradiation time. In order to clarify the reason for this, I analysed the photoreaction solution by LCMS in the next section.

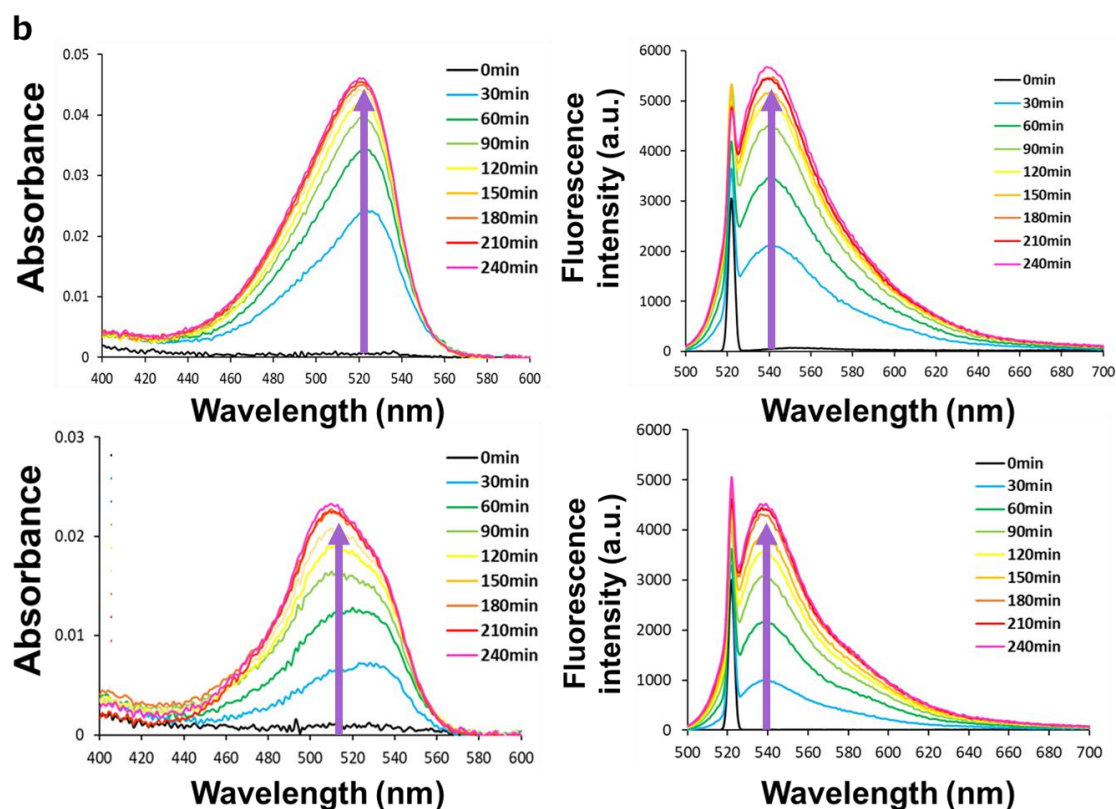


**Fig. 2.5.2** Change of absorbance (left) and fluorescence (right) spectra of 1  $\mu$ M solution of paSPiDER-1 (upper) and paSPiDER-2 (bottom) in 200 mM sodium phosphate buffer, pH 7.4, upon 405 nm light irradiation (18.3 or 19.3 mW/cm<sup>2</sup>) for 4 hours.

### 2.5.3 Reaction tracing with LC-MS

I analysed the photoreaction solution of paSPiDERs by LCMS and found that 4-CH<sub>2</sub>OH-HMDER and 4-CH<sub>2</sub>OH-HMDiEtR (water adducts of the respective (aza)quinone methide intermediates) were mainly produced, but *N*-dealkylated products were also formed by light irradiation, presumably via oxidative *N*-dealkylation<sup>47</sup> (Fig. 2.5.3). The photoreaction solution of paSPiDER-2 contained a higher percentage of *N*-

dealkylated by-products, which would explain the marked blue-shift in the absorption spectrum of paSPiDER-2 upon light irradiation, but I assumed that production of these *N*-dealkylated by-products would not be a problem for cell labelling.

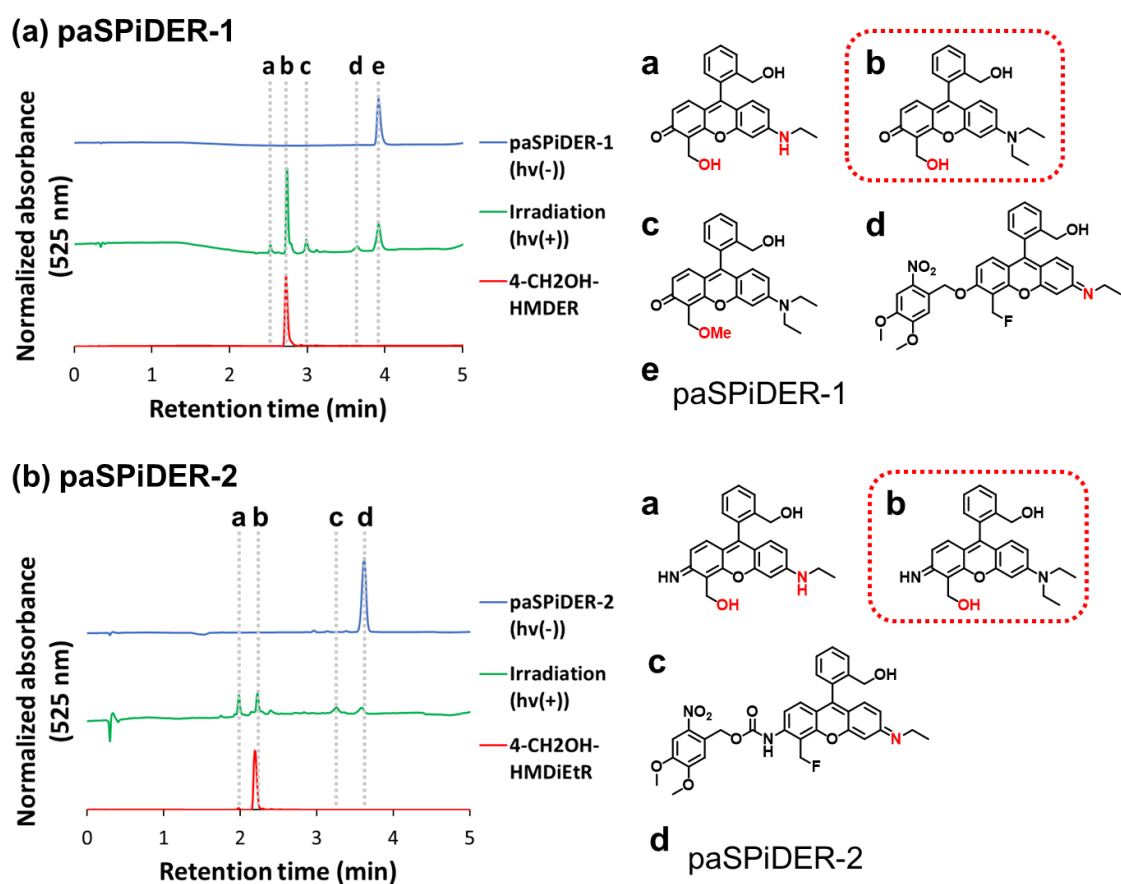


**Fig. 2.5.3** LC-MS analysis of photoreaction products of **paSPiDER-1** (a) and **paSPiDER-2** (b). 100  $\mu$ M solutions of paSPiDERs in 200 mM sodium phosphate buffer, pH 7.4, containing 1% DMSO (v/v), were irradiated at 405 nm (18.7 mW/cm<sup>2</sup> for 3 h for paSPiDER-1, and 18.3 mW / cm<sup>2</sup> for 1 h for paSPiDER-2). Absorbance at 525 nm was monitored. (top) Non-irradiated paSPiDER-1 or paSPiDER-2, (middle) the solutions after 405 nm light irradiation, (bottom) major hydrolysis products (4-CH<sub>2</sub>OH-HMDER or 4-CH<sub>2</sub>OH-HMDiEtR).

### 2.5.4 Protein labling

SDS-PAGE analysis of the photoreaction solution in the presence of bovine serum albumin (BSA) confirmed that photoactivated paSPiDERs can bind to BSA to produce fluorescent adducts (**Fig. 2.5.4**).

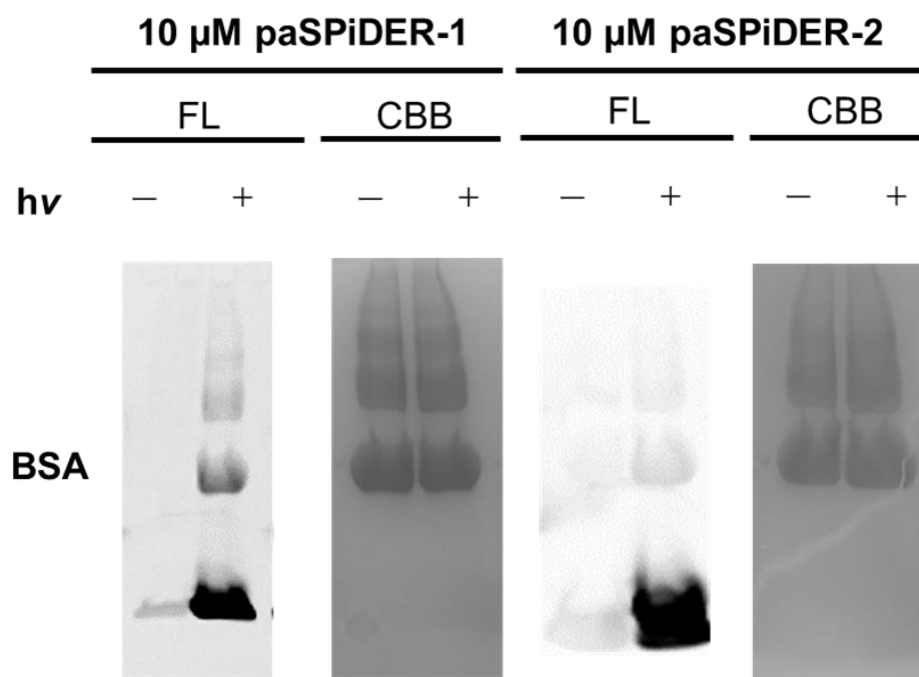


**Fig. 2.5.4** SDS-PAGE analysis of light irradiation samples contained with BSA and paSPiDERs. A solution of 1 mg/mL BSA and 100  $\mu$ M paSPiDER-1 or paSPiDER-2 in 200 mM sodium phosphate buffer, pH 7.4 containing 1% DMSO (v/v) was irradiated at 405 nm (18.7 mW/cm<sup>2</sup>) for 4 h, then subjected to SDS-PAGE analysis. Ex/Em = 497/520 nm.

## 2.6 Validation of probes *in cellulo*

### 2.6.1 Fluorescent cell labeling and resistance to fixation

Next, in order to determine whether paSPiDER-1 and paSPiDER-2 have cell membrane permeability and can function as PAFs in live cells, I applied them to cultured A549 cells (human lung adenocarcinoma-derived cell lines), followed by 405 nm laser light irradiation. I observed a significant fluorescence increase in cells in the light-irradiated region in both cases, demonstrating that the paSPiDERs are cell membrane permeable and do function as PAFs in live cells (**Fig. 2.6.1**). In cellulo photoactivation experiment does not require as much light exposure time as in vitro photoactivation experiments probably due to the higher intensity of activation light per unit and/or higher sensitivity of the confocal microscope. Further, the obtained fluorescence signals were resistant to 4% PFA fixation, which is known to induce cross-linking of intracellular components, as in the case of our previously reported SPiDER- $\beta$ Gal and 4-CH<sub>2</sub>F-HMDiEtR-gGlu. In contrast, fixation treatment with methanol, which is known to induce protein precipitation, reduced the fluorescence signal from paSPiDER-2, though the fluorescence signal from paSPiDER-1 was well maintained (**Fig. 2.6.1 right**). The results appeared to be independent of the passage number of the cells. As it was reported that MeOH fixation

leads to a more severe loss of cell components than PFA fixation<sup>48</sup>, this result suggests that activated paSPiDER-1 preferentially labels protein fractions resistant to MeOH fixation, as compared with paSPiDER-2, due to the difference in the generation rate or reactivity of quinone methide and azaquinone methide intermediates. I did not characterize what nucleophiles bind to the quinone methide intermediates, but it has been reported that quinone methide intermediates are trapped by cysteine thiol, lysine  $\epsilon$ -amine, and histidine imidazole<sup>49-51</sup>. Therefore, the intermediates produced from paSPiDERs would likely have been trapped by free nucleophilic amino acids, glutathione, and water, in addition to the protein fraction. In particular, azaquinone methide intermediates are predicted to be highly reactive and preferentially trapped by small molecule factors such as water and glutathione. Based on the above results, I focused on paSPiDER-1 for further experiments.

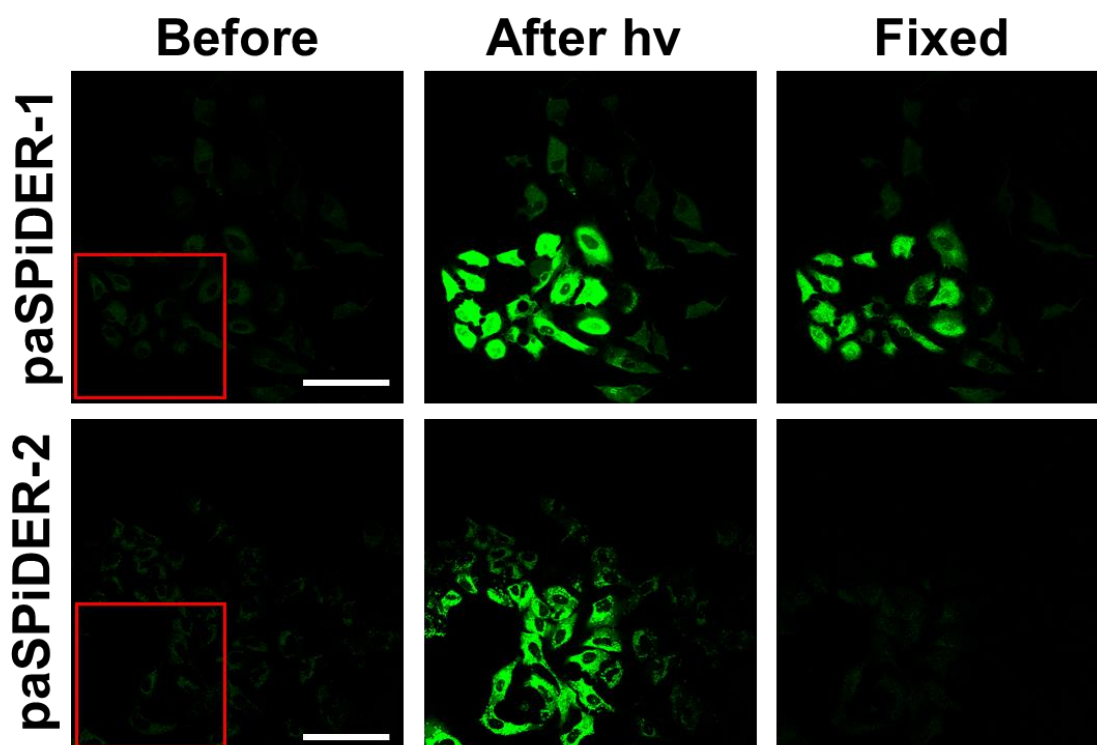


**Fig. 2.6.1** Fluorescent imaging of A549 cells treated with 10  $\mu$ M **paSPiDER-1** and **paSPiDER-2** for 1 h, followed by 405 nm light irradiation and MeOH fixation. (left) before light irradiation, (middle) after light irradiation, (right) after MeOH fixation for 15 min. Red square: 405 nm light-irradiated region. Ex/Em = 525 nm/535–595 nm. Scale bars, 100  $\mu$ m.



### 2.6.2 Long time imaging

In order to evaluate the practical utility of paSPiDER-1 for long-term imaging, I next examined whether the activated fluorescence signal of paSPiDER-1 can be tracked for 24 hours (**Fig. 2.6.2**). Although the fluorescence intensity gradually decreased, the cell region fluorescently labeled with paSPiDER-1 could be easily recognized even after 24 h. Further, I confirmed that the cells labeled with paSPiDER-1 divided normally (**Fig. 2.6.2, bottom**). These results suggested that paSPiDER-1 would be suitable for long-term cell tracking under certain measurement condition, but if more than 48 h is required, the further structural optimization needs to be performed to be better retained in cells.

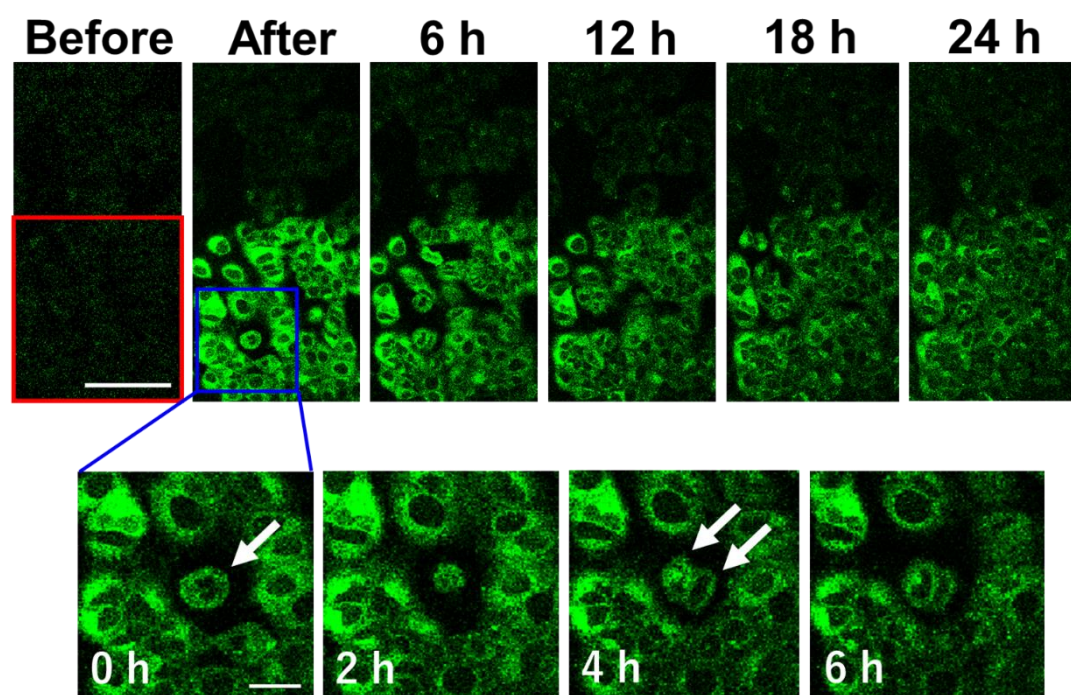


**Fig. 2.6.2** Time-lapse fluorescence imaging of A549 cells treated with 10  $\mu\text{M}$  **paSPiDER-1** for 1 h, followed by 405 nm light irradiation, for up to 24 h. Red square: 405 nm light-irradiated region. Ex/Em = 525 nm/535–595 nm. Scale bar, 100  $\mu\text{m}$ .

### 2.6.3 single cell labeling

Further, I evaluated whether selective cell labelling can be achieved by pinpoint light irradiation of single cells. Indeed, fluorescence activation was observed only in individually light-irradiated cells, enabling us to perform sequential cell labelling at single-cell resolution (**Fig. 2.6.3-1**).

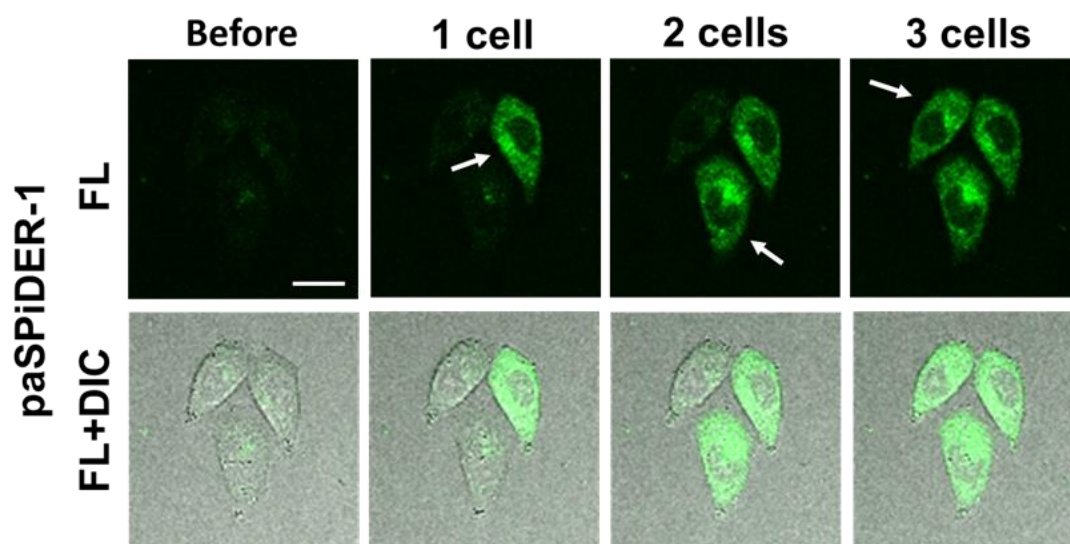


**Fig. 2.6.3-1** Single-cell fluorescent labeling of A549 cells treated with 10  $\mu$ M paSPiDER-1 for 1 h, and then successively irradiated with a 405 nm laser at the whole individual cell indicated by the white arrow in each panel. Ex/Em = 525 nm/535–595 nm. Scale bars, 20  $\mu$ m.

I also confirmed that the fluorescence signals activated locally in cells diffused throughout the cytoplasm, suggesting that fluorescence labelling of subcellular

regions with paSPiDER-1 would not be feasible (**Fig. 2.6.3-2**). In addition, based on these fluorescent cell imaging, I suppose that fluorescent hydrolysis product of paSPiDER-1 tends to localize in cytosol in cells.

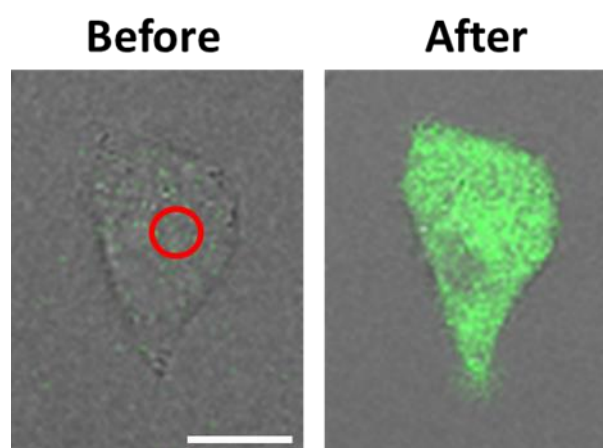


**Fig. 2.6.3-2** Fluorescence and DIC images of A549 cells treated with 10  $\mu\text{M}$  paSPiDER-1 for 1 h, and then successively irradiated with a 405 nm laser at the part of single-cell indicated by the red circle ( $n = 10$ ). The fluorescence image was captured 15 seconds after light irradiation. Ex/Em = 525 nm/535–595 nm. Scale bars, 20  $\mu\text{m}$ .

#### 2.6.4 Dark toxicity and phototoxicity

I further examined the toxicity of paSPiDER-1. First, I measured the dark toxicity of paSPiDER-1 compared to that of CellTracker<sup>TM</sup> Red CMTPX dye,

which is a commercially available cell-tracking dye with a thiol-reactive chloromethyl group, thus I used as a model comparison dye (**Fig. 2.6.4-1**). I confirmed that paSPiDER-1 did not show obvious cytotoxicity at the concentrations I used for cellular imaging, whereas CellTracker™ Red showed cytotoxicity in a concentration-dependent manner, owing to promiscuous labelling of intracellular nucleophiles such as proteins. These results demonstrated that the molecular design of paSPiDER-1 is effective to suppress dark toxicity compared to PAFs with thiol-reactive groups.

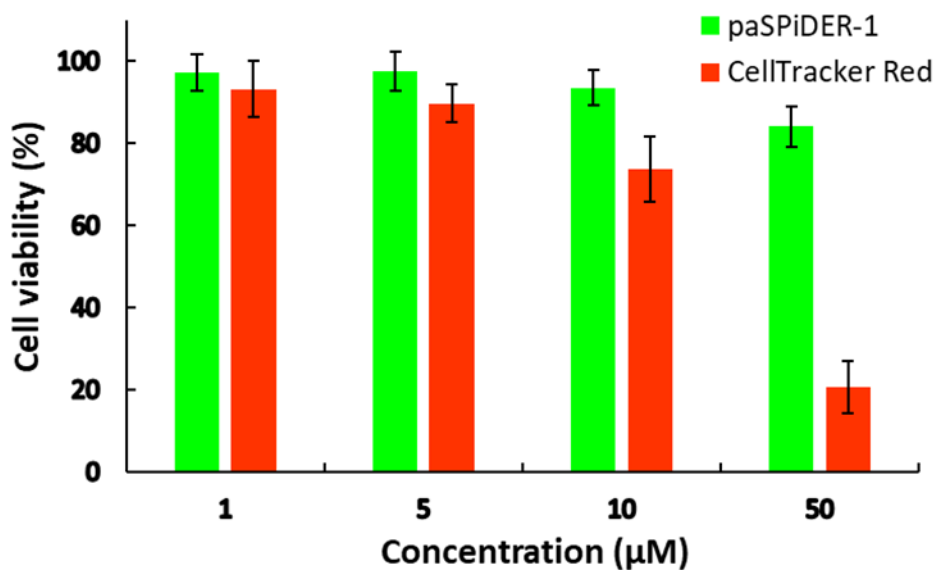


**Fig. 2.6.4-1** Comparison of the dark toxicity of paSPiDER-1 and CellTracker™ Red CMTPX dye to A549 cells. A549 cells were incubated with the indicated concentrations of paSPiDER-1 and CellTracker Red for 12 h at 37 °C under 5% CO<sub>2</sub>, and the cell viability was determined by CCK-8 assay. Data represent mean  $\pm$  s.d. from two independent experiments in quadruplicate.

Second, I evaluated the phototoxicity of paSPiDER-1 by staining paSPiDER-1-treated and light-irradiated cells with the cell-impermeant viability indicator, ethidium homodimer-1 (EthD-1), which stains only dead cells in red. I observed no marked staining with EthD-1 in paSPiDER-1-treated and light-irradiated cells for at least the following 15 h, whereas strong red staining was observed in fixed cells (**Fig. 2.6.4-2, -3**). These results indicate that the phototoxicity of paSPiDER-1 is low, and suggest that paSPiDER-1 would not substantially affect the physiological functions of live cells. Therefore, paSPiDER-1 should be suitable for live-cell fluorescence labelling experiments.

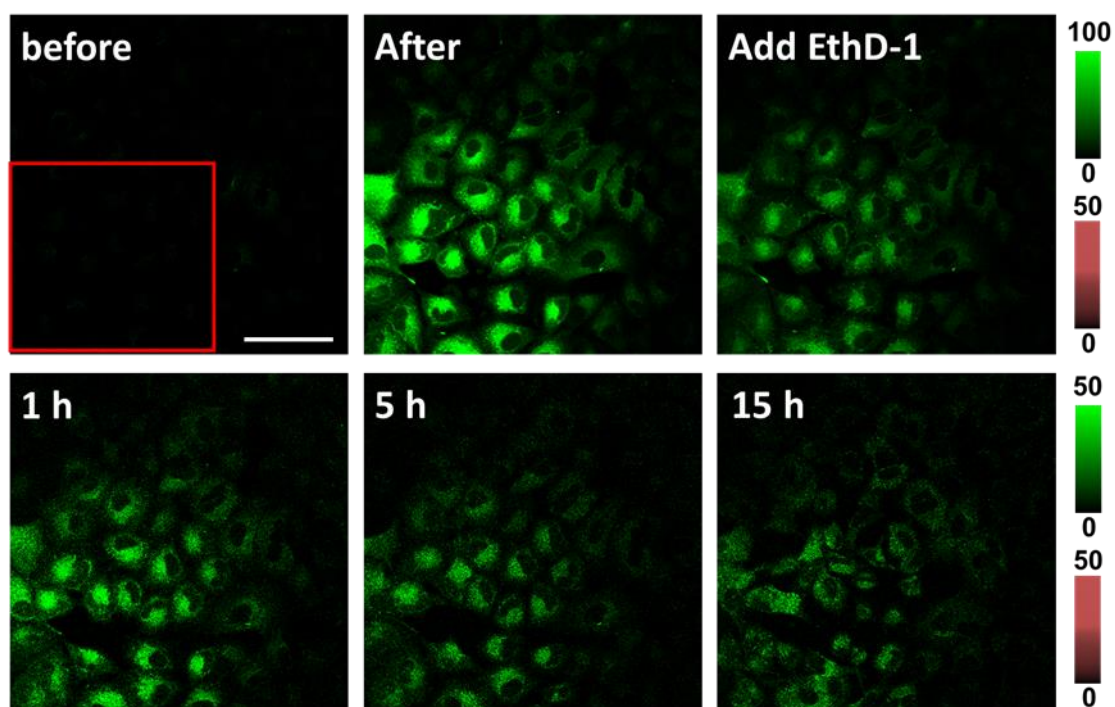


**Fig. 2.6.4-2** Evaluation of phototoxicity of paSPiDER-1. A549 cells were treated with 10  $\mu$ M paSPiDER-1 for 1 h, and cells in the region indicated by the red box were irradiated with a 405 nm laser. Then, fluorescence images were captured for 15 h after replacement of the medium with DMEM containing 2  $\mu$ M EthD-1. paSPiDER-1: ex/em = 520 nm/535–575 nm, EthD-1: ex/em = 561 nm/600–650 nm. Scale bars, 75  $\mu$ m.

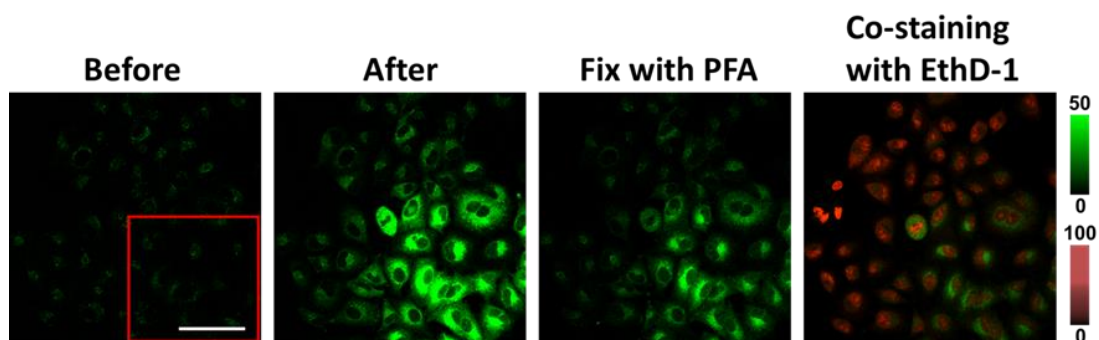


**Fig. 2.6.4-3.** EthD-1 staining of fixed cells. A549 cells were treated with 10  $\mu$ M paSPiDER-1 for 1 h, and cells in the region indicated by the red box were irradiated with a 405 nm laser. Then, the cells were fixed using 4% PFA solution for 15 min, and the solution was replaced with DMEM containing 2  $\mu$ M EthD-1. paSPiDER-1: ex/em = 520 nm/535–575 nm, EthD-1: ex/em = 561 nm/600–650 nm. Scale bars, 75  $\mu$ m.

## 2.7 Tissue imaging *ex vivo*

Finally, to confirm the applicability of paSPiDER-1 in live tissues, I performed *ex vivo* fluorescence labelling of *Drosophila melanogaster* tissues. I applied paSPiDER-1 to live larval wing disc, a precursor structure of a part of the adult thorax including the wing. After incubation for 30 min, 405 nm laser light irradiation significantly increased the fluorescence intensity only in the irradiated area, indicating that paSPiDER-1 works as a PAF in live tissues (Fig. 2.7). Further, the tissue was fixed with 4% PFA and subjected to immunostaining with anti-



phospho-histone H3 (PHH3) antibody as a model target marker. PHH3 was chosen because it is a common marker in humans and *Drosophila*. Although the fluorescence signal intensity derived from paSPiDER-1 was decreased following fixation, the fluorescently labelled cell region could still be clearly recognized, demonstrating the high compatibility of paSPiDER-1 with immunostaining.

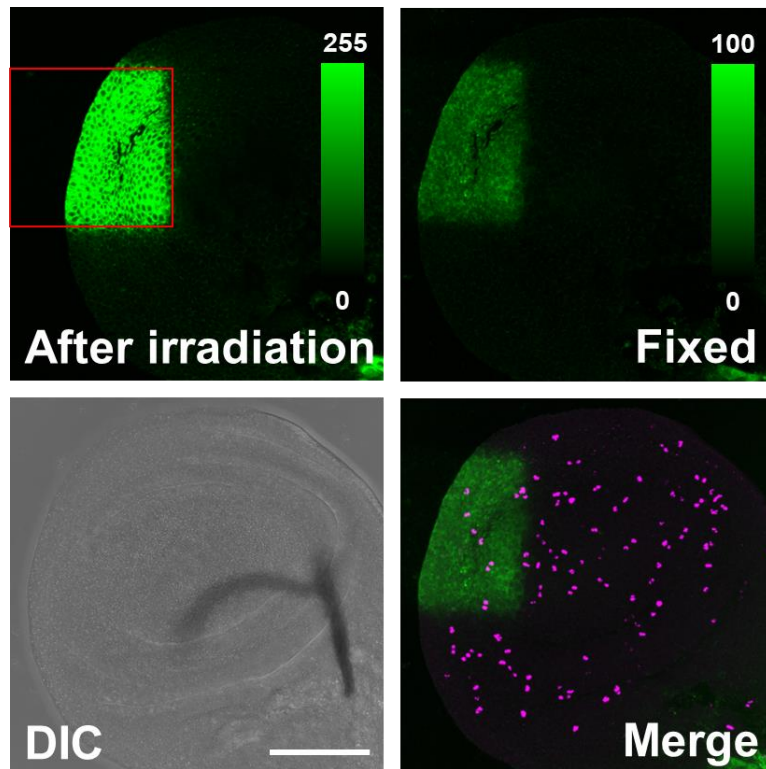


**Fig. 2.7** *Ex vivo* cell labeling of *Drosophila* tissue. *Drosophila* wing disc was treated with 50  $\mu$ M paSPiDER-1, followed by 405 nm light irradiation in the red square. Then, the tissue was fixed with 4% PFA and subjected to immunostaining with anti-phospho-histone H3 antibody (magenta). Ex/Em = 488 nm/500–550 nm. Scale bar, 75  $\mu$ m.

## **2.8 Brief summary**

I have developed cell-permeable PAFs, paSPiDERs, which were designed to show simultaneous activation of fluorescence and covalent binding ability to intracellular nucleophiles in response to light irradiation. Light activation of paSPiDER-1 produced fluorescence signals that were both resistant to MeOH fixation and durable, enabling long-term observation. In addition, selective cell labeling can be achieved at single-cell resolution. paSPiDER-1 also works on model organization, labelling is compatible with immunostaining.

## **Chapter 3**

### **Activatable orange fluorescent probes based on carborhodol scaffold**

## **Chapter 4**

## **Conclusion**

## 4.1 Overview

In this study, I developed new activatable fluorescent probes based on rhodol scaffold by using intramolecular spirocyclization as a mechanism of fluorescence control. In Chapter 2, I developed paSPiDERs, new photoactivatable fluorophores that simultaneously acquire intracellular retention and fluorescence activation upon light irradiation. In Chapter 3, I explored novel scaffold dyes and developed orange-emitting fluorescent probes for  $\beta$ -galactosidase, bGalBn3MeCOOHCR and bGalBnCOOHCR. These results clearly showed that rhodol-based fluorescence probes can be precisely designed, and these probes are compatible to live-cell imaging.

The paSPiDERs are novel photoactivatable fluorophores that can be easily used in a mixture of cells and tissues without genetic manipulation and cell toxicity. paSPiDERs are designed to acquire fluorescence and intracellular retention only after light irradiation. It is unique in terms of molecular design and has the potential to overcome the problems of conventional photoactivatable fluorophores of non-specific accumulation and cell toxicity to target/non-target cells, because it is possible to choose which cell to activate and to manipulate the production amount of reactive intermediates depending on the

irradiation time. This probe also can be used easily for cell lineage analysis as it does not require microinjection or genetic manipulation. In fact, I have confirmed that the probe shows large changes in absorption and fluorescence upon light irradiation, and that it can be labeled by intracellular nucleophilic molecules such as proteins by producing quinone methide intermediates. Furthermore, the results suggested that these photoactivatable fluorophores can be used to specific fluorescent labeling of target cells upon light irradiation and can be used for long-term observation and in combination with immunostaining.

## **4.2 Discussion and future prospect**

paSPiDERs enable fluorescent labeling and tracking of target cells, but also showing the limitation of a cell-tracking period and deep site imaging due to the wavelength of irradiation. For *in vivo* applications, if applied to zebrafish embryos after ovulation, it would be possible to track cell lineage to analyze cell fate from the early embryo because its body is relatively small and transparent and it grows for 48 hours into an adult. For bigger targets, two-photon uncaging would be useful to achieve deeper tissue labeling, but two-photon activation of paSPiDERs in their present forms would be difficult due to

the low sensitivity of DMNB caging groups to two-photon excitation<sup>45, 62</sup>. However, it would be possible to prepare paSPiDER analogues suitable for two-photon activation by replacing the DMNB moiety with other caging groups having a high two-photon cross-section. In addition, since paSPiDER-1 has a higher labeling rate with intracellular proteins, it is possible to use paSPiDER-1 labelling in combination with immunostaining.

## **Chapter 5**

### **Experimental section**

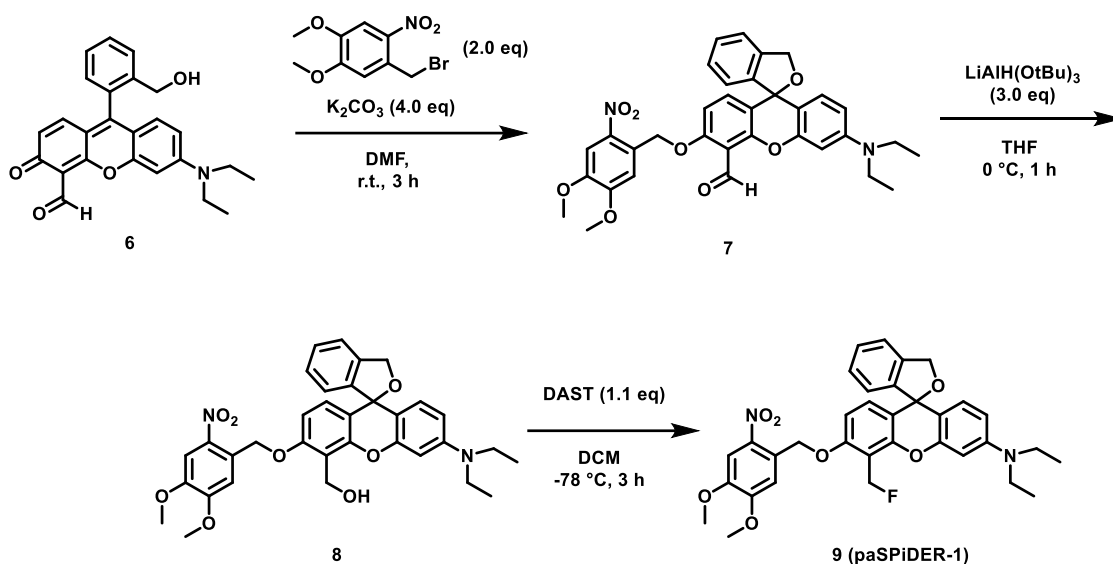


## Synthesis and characterization of compounds

### Materials and general information

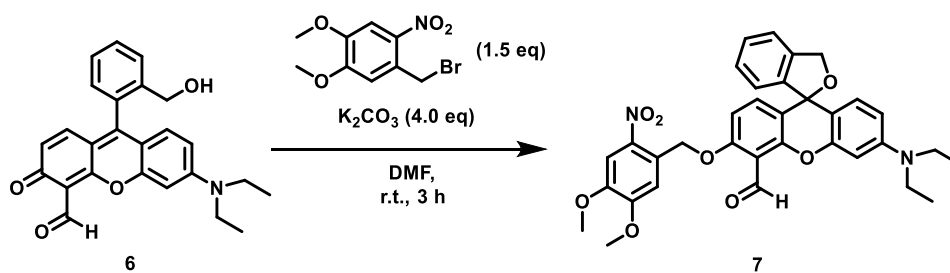
All chemical reagents and dry solvents for synthesis were purchased from commercial suppliers (Wako Pure Chemical, Tokyo Chemical Industries, Sigma-Aldrich Japan) and were used without further purification. The composition of mixed solvents is given as volume ratio (v/v). Dimethyl sulfoxide (DMSO, fluorometric grade) used for the spectrometric measurements was purchased from Dojindo.  $^1\text{H}$  and  $^{13}\text{C}$  nuclear magnetic resonance (NMR) spectra were recorded on an AVANCE III 400 Nanobay (Bruker, 400 MHz for  $^1\text{H}$  NMR, 101 MHz for  $^{13}\text{C}$  NMR). Mass spectra (MS, ESI-TOF) were measured with a MicroTOF (Bruker). High-resolution MS (HRMS) was measured using sodium formate as an external standard. Flash chromatographic purifications were performed on an automated silica gel flash column chromatography system YFLC AI-580 (Yamazen). Preparative reversed-phase HPLC using an Inertsustain C18 4.6 mm x 150 mm column (GL Science) or an Inertsil ODS-3 20 mm x 250 mm column (GL Science) was performed on a PU-2080 system equipped with a MD-2010 detector (JASCO) or a PU-2087 system equipped with a MD-2010 detector (JASCO). Solvent A: 99%  $\text{H}_2\text{O}$ , 1%  $\text{CH}_3\text{CN}$  (TFA 0.1%). B: 99%  $\text{CH}_3\text{CN}$  and 1%  $\text{H}_2\text{O}$ .

## Chapter 2 :



**Scheme 5.1.** Synthetic scheme of paSPiDER-1.

### 4-CHO-caged HMDER, 7

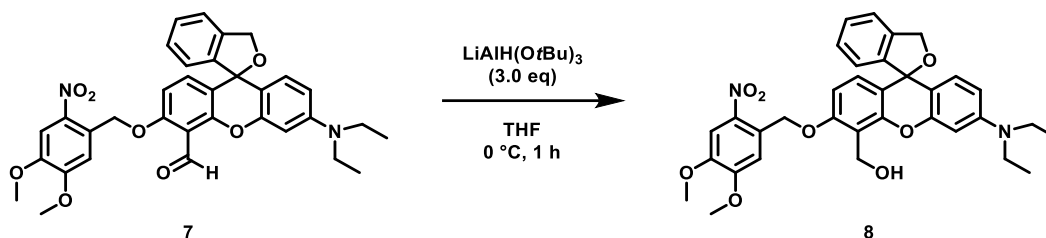


**Scheme 5.2.** Synthesis of 4-CHO-caged HMDER 7.

Compound **6** was synthesized as previously described<sup>36</sup>. To a solution of compound **1**

(104 mg, 0.25 mmol) in dry DMF (3 mL), potassium carbonate (173 mg, 1.25 mmol), 4,5-dimethoxy-2-nitrobenzyl bromide (143 mg, 0.50 mmol), and a small amount of sodium sulfate were added, and the solution was stirred at r.t. for 3 h. Then, the reaction mixture was evaporated and the residue was dissolved in water. The resulting solution was extracted with CH<sub>2</sub>Cl<sub>2</sub> (3 x), and the combined organic layer was evaporated. The residue was purified by silica gel flash column chromatography (hexane/EtOAc = 67/33) to obtain the desired product **7** as a red solid (99.8 mg, y. 67%). A sample was identified by <sup>1</sup>H NMR (400 MHz, CDCl<sub>3</sub>): δ 1.17 (6H, t, *J* = 7.0 Hz), 3.36 (4H, q, *J* = 7.0 Hz), 3.96 (3H, s), 4.25 (3H, s), 5.25 (1H, d, *J* = 12.4 Hz), 5.29 (1H, d, *J* = 12.4 Hz), 5.50 (2H, s), 6.42 (1H, dd, *J* = 8.8, 2.6 Hz), 6.47 (1H, d, *J* = 2.6 Hz), 6.77 (1H, d, *J* = 8.8 Hz), 6.83 (1H, d, *J* = 8.8 Hz), 6.94 (1H, d, *J* = 7.6 Hz), 7.16 (1H, d, *J* = 8.8 Hz), 7.28 (1H, m), 7.38 (2H, m), 7.76 (1H, s), 8.27 (1H, s), 10.93 (1H, s); <sup>13</sup>C NMR (101 MHz, CDCl<sub>3</sub>): δ 12.6, 44.5, 56.4, 57.3, 67.9, 71.9, 83.3, 97.8, 107.5, 107.7, 109.0, 110.7, 110.9, 112.6, 119.0, 120.8, 123.9, 128.3, 128.5, 129.2, 129.5, 136.6, 138.2, 139.6, 144.4, 147.8, 149.0, 151.2, 154.5, 154.8, 158.3, 188.5; HRMS (ESI<sup>+</sup>): calcd for [M+Na]<sup>+</sup>, 619.20509; found, 619.20507 (0.02 mmu).

### 4-CH<sub>2</sub>OH-caged HMDER, 8

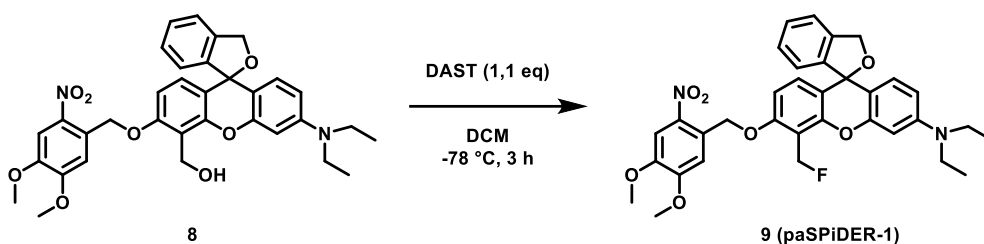


#### **Scheme 5.3. Synthesis of 4-CH<sub>2</sub>OH-caged HMDER 8.**

Compound **7** (20 mg, 0.0 mmol) was dissolved in dry THF (4 mL) and the solution was stirred at 0 °C. 1.0 M LiAlH(O $t$ Bu)<sub>3</sub> in THF (0.5 mL) was added dropwise and stirring was continued at 0 °C for 1 h. Saturated NH<sub>4</sub>Cl aqueous solution (3 mL) was added to the solution on ice to quench the reaction. EtOAc (7 mL) was added and the solution was stirred at room temperature for 1 h, then the organic phase was separated. Saturated potassium sodium tartrate aqueous solution and CH<sub>2</sub>Cl<sub>2</sub> were added to the aqueous phase. The reaction mixture was stirred, and the organic phase was separated (2 x). The combined organic phase was evaporated, and the residue was purified by silica gel flash column chromatography (CH<sub>2</sub>Cl<sub>2</sub>/EtOAc = 98/2) to obtain the desired product **8** as an orange solid. A sample was identified by <sup>1</sup>H NMR (400 MHz, CDCl<sub>3</sub>):  $\delta$  1.17 (6H, t,  $J$  = 7.0 Hz), 3.36 (4H, q,  $J$  = 7.0 Hz), 3.96 (3H, s), 3.98 (3H, s), 5.14 (2H, s), 5.20 (1H, d,  $J$  = 12.4 Hz), 5.24 (1H, d,  $J$  = 12.4 Hz), 5.53 (2H, s), 6.40 (1H, dd,  $J$  = 8.8, 2.6 Hz), 6.46 (1H, d,  $J$  = 2.6 Hz), 6.64 (1H, d,  $J$  = 8.8 Hz), 6.75 (1H, d,  $J$  = 8.8 Hz), 6.85 (1H, d,  $J$  = 8.8 Hz),

6.93 (d, 1H,  $J = 7.6$  Hz), 7.27 (1H, m), 7.35 (2H, m), 7.42 (1H, s), 7.75 (1H, s);  $^{13}\text{C}$  NMR (101 MHz,  $\text{CDCl}_3$ ):  $\delta$  12.7, 44.5, 54.9, 56.6, 67.5, 71.6, 77.3, 83.9, 97.8, 107.6, 108.1, 108.6, 109.6, 111.3, 116.0, 119.3, 120.7, 124.1, 128.1, 128.3, 129.2, 129.6, 129.8, 139.1, 139.8, 144.6, 148.0, 148.9, 150.0, 151.9, 154.2, 156.9; HRMS (ESI<sup>+</sup>): calcd for  $[\text{M}+\text{H}]^+$ , 599.23879; found, 599.23958 (0.8 mmu).

#### **paSPiDER-1, 9.**

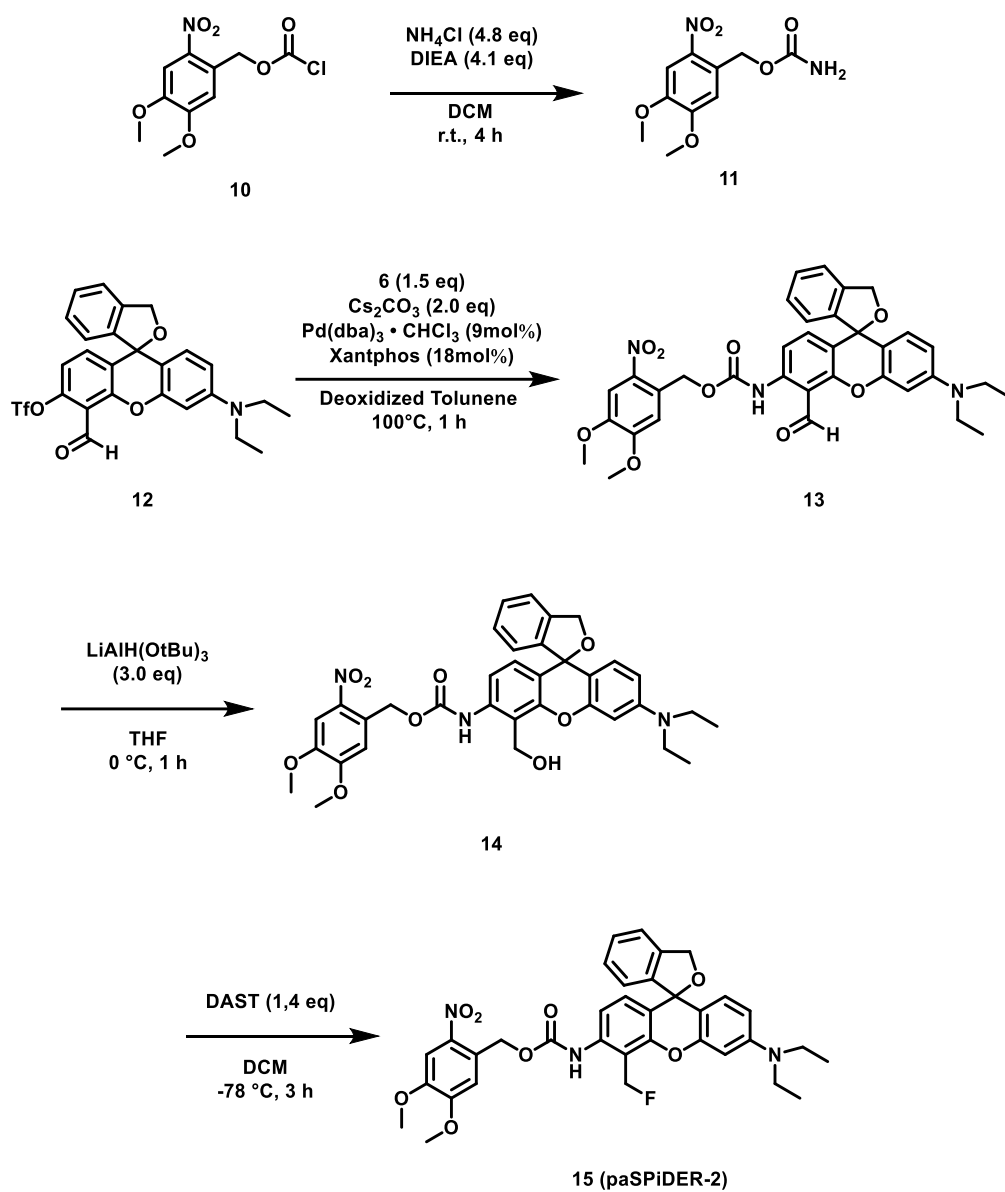


#### **Scheme 5.4. Synthesis of paSPiDER-1 9.**

Compound **8** (10 mg, 0.017 mmol) was dissolved in dry  $\text{CH}_2\text{Cl}_2$  (1 mL), and a solution of DAST (3.3  $\mu\text{L}$ , 0.018 mmol) in  $\text{CH}_2\text{Cl}_2$  was added dropwise at  $-78$   $^\circ\text{C}$ . The mixture was stirred at  $-78$   $^\circ\text{C}$  for 3 h. MeOH and  $\text{H}_2\text{O}$  were added at r.t., and the resulting mixture was extracted with  $\text{CH}_2\text{Cl}_2$  (3 x). The combined organic phase was evaporated, and the residue was purified by silica gel flash column chromatography (Hexane/EtOAc = 67/33) and HPLC (A/B = 10/90 to 90/10) to obtain paSPiDER (**9**) as a red solid (2.5 mg, y. 25%).

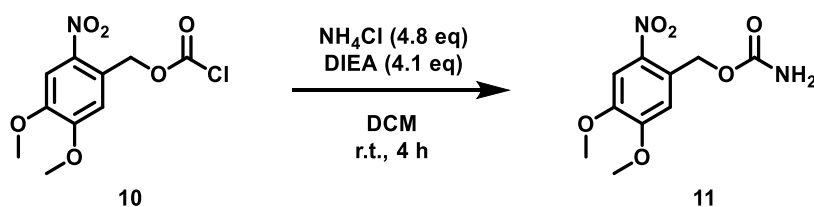
A sample was identified by  $^1\text{H}$  NMR (400 MHz,  $\text{CDCl}_3$ ):  $\delta$  1.17 (6H, t,  $J = 7.0$  Hz), 3.36

(4H, q,  $J = 7.0$  Hz), 3.96 (3H, s), 3.97 (3H, s), 5.22 (1H, d,  $J = 12.4$  Hz), 5.25 (1H, d,  $J = 12.4$  Hz), 5.56 (2H, s), 5.90 (1H, dd,  $J = 48.4, 16.4$  Hz), 5.92 (1H, dd,  $J = 48.4, 16.4$  Hz), 6.40 (1H, dd,  $J = 8.8, 2.6$  Hz), 6.48 (1H, d,  $J = 2.6$  Hz), 6.65 (1H, d,  $J = 8.8$  Hz), 6.75 (1H, d,  $J = 8.8$  Hz), 6.92 (1H, d,  $J = 7.8$  Hz), 6.94 (1H, dd,  $J = 8.9, 2.6$  Hz), 7.27 (1H, m), 7.36 (2H, m), 7.49 (1H, s), 7.75 (1H, s);  $^{13}\text{C}$  NMR (101 MHz,  $\text{CDCl}_3$ ):  $\delta$  12.7, 44.5, 56.4, 56.6 ( $J_{\text{CF}} = 1.01$  Hz), 67.0, 71.7, 74.1 ( $J_{\text{CF}} = 161.6$  Hz), 83.8, 97.9, 107.1 ( $J_{\text{CF}} = 2.939$  Hz), 108.0, 108.6, 109.5, 111.1 ( $J_{\text{CF}} = 10.1$  Hz), 111.2, 119.2 ( $J_{\text{CF}} = 2.868$  Hz), 120.7, 124.1, 128.1, 128.4, 129.4, 129.5, 131.8 ( $J_{\text{CF}} = 4.272$  Hz), 138.9, 139.7, 144.7, 147.9, 148.9, 150.7 ( $J_{\text{CF}} = 2.989$  Hz), 151.8, 154.4, 157.5 ( $J_{\text{CF}} = 2.80$  Hz); HRMS (ESI<sup>+</sup>): calcd for  $[\text{M}+\text{H}]^+$ , 601.23446; found, 601.23339 (1.1 mmu).



**Scheme 5.5.** Synthetic scheme of paSPiDER-2.

**4,5-Dimethoxy-2-nitrobenzyl amideformate, 11.**

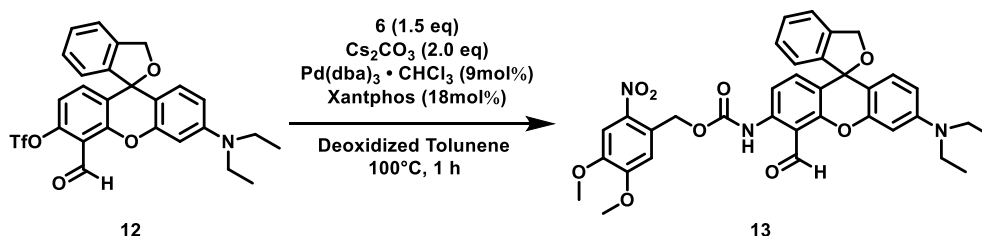


**Scheme 5.6. Synthesis of 4,5-dimethoxy-2-nitrobenzyl amideformate, 6.**

To a solution of 4,5-dimethoxy-2-nitrobenzyl chloroformate **10** (434 mg, 1.7 mmol) in dichloromethane (10 mL), ammonium chloride (439 mg, 8.2 mmol), and N,N-diisopropylethylamine (1.2 mL, 6.9 mmol) were added, and the mixture was stirred vigorously at r.t. under an Ar atmosphere for 4 h. A mixed solvent (H<sub>2</sub>O 5 mL, iPrOH 1.5 mL, and dichloromethane 3.5 mL) was added at r.t., and the solution was stirred for 10 min, then filtered and evaporated. The residue was purified by silica gel flash column chromatography (hexane/EtOAc = 67/33) to obtain the desired product **11** as a yellow solid (308 mg, y. 71%). A sample was identified by <sup>1</sup>H NMR (400 MHz, DMSO-d<sub>6</sub>): δ 3.87 (3H, s), 3.90 (3H, s), 5.29 (2H, s), 6.62 (1H, br), 6.91 (1H, br), 7.19 (1H, s), 7.69 (1H, s). <sup>13</sup>C NMR (101 MHz, DMSO-d<sub>6</sub>): δ 56.0, 56.2, 61.9, 108.0, 110.5, 127.9, 139.3, 147.6, 153.2, 156.1; HRMS (ESI<sup>+</sup>): calcd for [M+Na]<sup>+</sup>, 279.05876; found, 279.05745 (1.3 mmu).



### 4-CHO-caged HMDiEtR, 13.



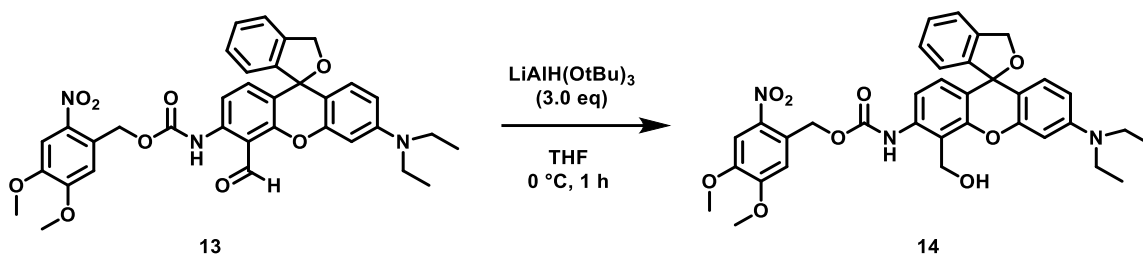
**Scheme 5.7. Synthesis of 4-CHO-caged HMDiEtR 13.**

Compound **12** was synthesized as previously described<sup>37</sup>. To a solution of compound **7** (100 mg, 0.19 mmol) in deoxygenated toluene (5 mL), cesium carbonate (122 mg, 0.38 mmol), 4,5-dimethoxy-2-nitrobenzyl amideformate **6** (72 mg, 0.28 mmol), xantphos (20 mg, 0.033 mmol), and tris(dibenzylideneacetone)dipalladium(0) chloroform adduct (18 mg, 0.017 mol) were added. The solution was stirred vigorously at  $100^\circ\text{C}$  under an Ar atmosphere for 1.5 h, then filtered and evaporated. The residue was purified by silica gel flash column chromatography (Hexane/EtOAc = 67/33) to obtain the desired product **13** as a yellow solid (85 mg, y. 71%). A sample was identified by  $^1\text{H}$  NMR (400 MHz,  $\text{CDCl}_3$ ):  $\delta$  1.17 (6H, t,  $J = 7.0$  Hz), 3.36 (4H, q,  $J = 7.0$  Hz), 3.96 (3H, s), 4.25 (3H, s), 5.25 (1H, d,  $J = 12.4$  Hz), 5.29 (1H, d,  $J = 12.4$  Hz), 5.50 (2H, s), 6.42 (1H, dd,  $J = 8.8, 2.6$  Hz), 6.47 (1H, d,  $J = 2.6$  Hz), 6.77 (1H, d,  $J = 8.8$  Hz), 6.83 (1H, d,  $J = 8.8$  Hz), 6.94 (1H, d,  $J = 7.6$  Hz), 7.16 (1H, d,  $J = 8.8$  Hz), 7.28 (1H, m), 7.38 (2H, m), 7.76 (1H, s), 8.27

(1H, s), 10.93 (1H, s); HRMS (ESI<sup>+</sup>): calcd for [M+Na]<sup>+</sup>, 662.21090; found, 662.21090

(0.0 mDa).

#### **4-CH<sub>2</sub>OH-caged HMDiEtR, 14.**

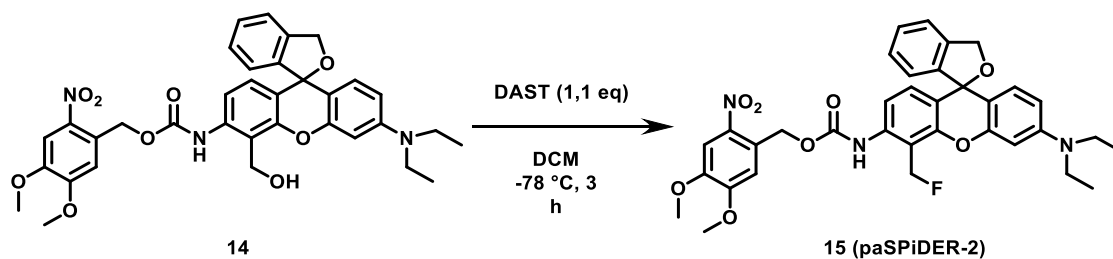


#### **Scheme 5.8. Synthesis of 4-CH<sub>2</sub>OH-caged HMDiEtR 14.**

Compound **13** (85 mg, 0.13 mmol) was dissolved in dry THF (5 mL) and the solution was stirred at 0 °C. 1.0 M  $\text{LiAlH}(\text{OtBu})_3$  in THF (0.5 mL) was added dropwise and the resulting solution was stirred at 0 °C for 1 h. Saturated  $\text{NaHCO}_3$  aqueous solution (3 mL) was added on ice to quench the reaction. EtOAc (7 mL) was added and the mixture was stirred at room temperature for 1 h, then the organic phase was separated. Saturated potassium sodium tartrate aqueous solution and  $\text{CH}_2\text{Cl}_2$  were added to the aqueous phase. The mixture was stirred, and the organic phase was separated (2 x). The combined organic phase was evaporated and the residue was purified by silica gel flash column

chromatography (hexane/EtOAc = 70/30) to obtain the desired product **14** as an orange solid (85 mg, y. 99%). A sample was identified by  $^1\text{H}$  NMR (400 MHz,  $\text{CDCl}_3$ ):  $\delta$  1.16 (6H, t,  $J = 7.0$  Hz), 3.34 (4H, q,  $J = 7.0$  Hz), 3.94 (3H, s), 3.96 (3H, s), 4.91 (2H, s), 5.22 (1H, d,  $J = 12.5$  Hz), 5.26 (1H, d,  $J = 12.5$  Hz), 5.58 (1H, d,  $J = 14.1$  Hz), 5.64 (1H, d,  $J = 14.1$  Hz), 6.38 (1H, s), 6.42 (1H, d,  $J = 8.4$  Hz), 6.72 (d, 1H,  $J = 8.8$  Hz), 6.79 (1H, d,  $J = 8.4$  Hz), 6.85 (1H, d,  $J = 8.8$  Hz), 6.90 (1H, d,  $J = 7.6$  Hz), 7.25 (1H, m), 7.35 (2H, m), 7.52 (1H, br), 7.70 (1H, s), 8.30 (1H, s); HRMS (ESI $^+$ ): calcd for  $[\text{M}+\text{H}]^+$ , 642.24461 found, 662.24551 (0.9 mDa).

#### paSPiDER-2, 15.



**Scheme 5.9. Synthesis of paSPiDER-2 15.**

Compound **14** (85 mg, 0.13 mmol) was dissolved in dry  $\text{CH}_2\text{Cl}_2$  (1 mL), and a solution of DAST (8.8  $\mu\text{L}$ , 0.066 mmol) in  $\text{CH}_2\text{Cl}_2$  was added dropwise at  $-78\text{ }^\circ\text{C}$ . The mixture

was stirred at -78 °C for 3 h. MeOH and H<sub>2</sub>O were added at r.t., and the resulting mixture was extracted with CH<sub>2</sub>Cl<sub>2</sub> (3 x). The combined organic phase was evaporated, and the residue was purified by silica gel flash column chromatography (hexane/EtOAc = 67/33) and HPLC (A/B = 90/10 to 10/90) to obtain paSPiDER-2 **15** as a red solid (12 mg, y. 14%). A sample was identified by <sup>1</sup>H NMR (400 MHz, CDCl<sub>3</sub>): δ 1.21 (6H, t, *J* = 7.1 Hz), 3.58 (4H, q, *J* = 7.0 Hz), 3.96 (3H, s), 3.97 (3H, s), 5.16 (2H, br), 5.63 (2H, s), 5.91 (1H, dd, *J* = 48.1, 19.4 Hz), 5.95 (1H, dd, *J* = 48.1, 19.4 Hz), 6.93 (1H, d, *J* = 7.5 Hz), 7.04 (1H, s), 7.10 (1H, dd, *J* = 8.8, 2.1 Hz), 7.13 (1H, d, *J* = 6.3 Hz), 7.20 (1H, d, *J* = 8.8 Hz), 7.27 (1H, m), 7.34 (1H, m), 7.45 (2H, m), 7.57 (1H, br), 7.74 (1H, s), 7.84 (1H, m); HRMS (ESI<sup>+</sup>): calcd for [M+H]<sup>+</sup>, 644.24027; found, 644.24179 (1.5 mDa).

## Methods

### Spectral measurements

UV-visible absorption spectra were measured using a UV-2450 spectrophotometer (Shimadzu), and fluorescence spectra were measured using a F-7000 fluorescence spectrophotometer (Hitachi). The probes were first dissolved in DMSO (fluorometric grade, Dojindo) to obtain stock solutions. Absolute fluorescence quantum efficiency was determined with an absolute PL quantum yield spectrometer, Quantaaurus-QY (Hamamatsu Photonics). For photoirradiation experiments in vitro, probe solutions (1  $\mu$ M) in 200 mM sodium phosphate buffer, pH 7.4, in a quartz cuvette were illuminated at 405 nm (18.3 or 19.3 mW/cm<sup>2</sup>) using a Xe lamp (Asahi Spectra Inc., MAX-303) equipped with a 405 nm bandpass filter (FWHM 10 nm) with stirring at room temperature. The absorption and fluorescence spectra were recorded every 15 or 30 minutes.

### Determination of $pK_{\text{cycl}}$ or $pK_{\text{a}}$ values of compounds

Absorption and fluorescence emission spectra of compounds were measured in 200 mM sodium phosphate buffer at different pH values, containing <1% (v/v) DMSO as a cosolvent. For compounds with  $n$  acid-base equilibria ( $n = 1$  or  $2$ ), pH profiles of absorbance (Abs) or fluorescence intensity (FI) were fitted to the following formula to

determine  $pK_a$  values.

$$\text{Abs or FI} = \frac{c_0 + \sum_{k=1}^n c_k \cdot 10^{k \cdot \text{pH} - \sum_{l=1}^k pK_{a,l}}}{1 + \sum_{k=1}^n 10^{k \cdot \text{pH} - \sum_{l=1}^k pK_{a,l}}}$$

( $pK_{a,1} < pK_{a,2} < \dots < pK_{a,n}$ ;  $c_n = \text{constant}$ ).

### **LC-MS analysis of photoreaction products**

A solution of probes in 200 mM sodium phosphate buffer, pH 7.4, containing 0.1% DMSO as a co-solvent was irradiated at room temperature for 3 h. LC-MS analyses of the photoreaction solution were performed on a Waters Acquity UPLC (H class)/QDa quadrupole MS analyzer equipped with an Acquity UPLC BEH C18 column (Waters). Eluent A (H<sub>2</sub>O containing 0.1 % formic acid) and eluent B (acetonitrile) were used for UPLC analyses.

### **SDS-PAGE of photoreaction products in the presence of BSA**

Solutions of BSA (1 mg/ml) and probes in 200 mM sodium phosphate buffer, pH 7.4 were incubated and irradiated for 5 h. SDS-PAGE analyses were performed using Mini-PROTEAN TGX Gels (Bio-Rad). Fluorescence images of the gels were obtained on an Image Quant LAS 4000 (GE Healthcare) with a 497 nm LED for excitation and a 520 nm long pass filter for emission. The gels were stained with Coomassie brilliant blue (CBB) solution.

### **Cell line and culture**

A549 and HEK293/HEK293-LacZ(+) cells were cultured  $5.0 \times 10^4$  cells in DMEM (Wako) containing 10 % fetal bovine serum (FBS), 100 U/mL penicillin, and 100  $\mu$ g/mL streptomycin at 37 °C in 5% CO<sub>2</sub>.

### **Confocal imaging of cells**

Cells were seeded  $1.0 \times 10^3$  cells/well on 8-chamber plates (Ibidi,  $\mu$ -slide) and cultured overnight. The medium was replaced with probes in phenol red-free DMEM or HBSS(-), and the cells were further incubated for 1 hour at 37 °C under 5% CO<sub>2</sub>.

As for photoactivatable probes, The cells were photo-irradiated with a 405 nm laser under a confocal microscope (for single-cell labeling : 5%, 25 sec for paSPiDER-1, 50%, 20 sec for paSPiDER-2, others : 100%, 30 sec). For fixation, the light-irradiated cells were incubated with 4% paraformaldehyde (PFA) or MeOH for 15 minutes at room temperature and washed with PBS. For evaluation of phototoxicity, the medium was replaced with DMEM containing 2  $\mu$ M ethidium homodimer-1 (EthD-1). DIC and fluorescence images were acquired with a confocal fluorescence microscope (for single-cell labeling : TCS SP5 X, others : TCS SP8 STED, Leica) equipped with a white-light laser, a 405 nm laser and an objective lens (for single-cell labeling : HCX PL APO CS

63x/1.40 Oil, others : HCX PL APO CS 40x/1.25 Oil, Leica). For time-lapse imaging, fluorescence images were captured every 1 h for 24 h. For evaluation of phototoxicity, excitation and emission wavelengths were 520 nm/535–575 nm for paSPiDER-1, 561 nm/600–650 nm for EthD-1. Others, ex/em = 525 nm/535-595 nm for paSPiDERs, ex/em = 575 nm/595-695 nm for bGalBnCOOHCR and bGalBn3MeCOOHCR.

### **Cell viability assay**

A549 cells were seeded  $1.0 \times 10^4$  cells/well in a plastic-bottomed 96-well plate and cultured overnight. The medium was exchanged to fresh medium containing paSPiDER-1 or CellTracker<sup>TM</sup> Red CMTPX dye (product number C34552, ThermoFisher) at various concentrations, containing 1% DMSO as a cosolvent, followed by incubation for 12 h at 37°C. The medium in each well was replaced with 100  $\mu$ L of fresh medium. The cells were further incubated in medium containing 10% Cell Counting Kit-8 (Dojindo), and the absorbance at 450 nm was measured using an Envision plate reader (Perkin Elmer) to determine the cell viability. Values from wells containing cells without dyes were taken as representing 100% cell viability.



### **Imaging of *Drosophila* wing disc**

Wing imaginal discs of third-instar larvae from *Drosophila melanogaster* Canton S were dissected in PBS. Dissected tissues were incubated with 50  $\mu$ M paSPiDER-1 in Schneider's *Drosophila* Medium (Gibco, 21720001) supplemented with 10% FBS for 30 min at room temperature, then flush-washed with PBS, mounted on a glass-bottomed dish (Matsunami, D111300), and incubated with the medium. UV irradiation was performed using an Leica SP8 microscope with a 405 nm laser at 20% intensity for 15 sec. The irradiated tissue was fixed in 4 % PFA for 30 min. After washing with PBST (0.1 % Triton-X100), the tissue was incubated with blocking buffer (PBST (0.1% Triton-X100) with 5 % normal donkey serum) for 30 min, followed by incubation with anti-phosphohistone (S28) H3 rat monoclonal antibody (Abcam, ab10543) diluted 1:200 in the blocking buffer for 60 minutes. After washing with PBST, second antibody anti-rat IgG 633 (Thermo Fisher Scientific, A-21094) was used to visualise the pH3 signal under a Leica SP8 microscope. Excitation/emission wavelengths were 488 nm/500-550 nm for paSPiDER-1 and 633 nm/645-695 nm for second antibody anti-rat IgG 633, respectively.

## Reference

1. Weissleder, R.; Pittet, M. J., Imaging in the era of molecular oncology. *Nature* **2008**, *452* (7187), 580-9.
2. Baeyer, A., Ueber eine neue Klasse von Farbstoffen. *Berichte der deutschen chemischen Gesellschaft* **2006**, *4* (2), 555-558.
3. Coons, A. H., Creech, H., Jones, R. & Berliner, E., The demonstration of pneumococcal antigen in tissues by the use of fluorescent antibody. *J. Immunol.* **1942**, *45*, 159–170.
4. Loudet, A. B., K., BODIPY dyes and their derivatives: syntheses and spectroscopic properties. *Chem. Rev.* **2007**, *107*, 4891–4932.
5. Smith, L. M. e. a., Fluorescence detection in automated DNA sequence analysis. *Nature* **1986**, *321*, 674-679.
6. Lee, L. G. e. a., DNA sequencing with dye-labeled terminators and T7 DNA polymerase: effect of dyes and dNTPs on incorporation of dye-terminators and probability analysis of termination fragments. *Nucleic Acids Res.* **1992**, *20*, 2471-2483.
7. Mujumdar, R. B., Ernst, L. A., Mujumdar, S. R., Lewis, C. J. &

Waggoner, A.S., Cyanine dye labeling reagents: Sulfoindocyanine

succinimidyl esters. *Bioconjugate Chem.* **1993**, *4*, 105-111.

8. Panchuk-Voloshina, N. e. a., Alexa Dyes, a series of new fluorescent dyes that yield exceptionally bright, photostable conjugates. *J. Histochem. Cytochem.* **1999**, *47*, 1179–1188.

9. Tebo, A. G.; Moeyaert, B.; Thauvin, M.; Carlon-Andres, I.; Boken, D.; Volovitch, M.; Padilla-Parra, S.; Dedecker, P.; Vriz, S.; Gautier, A., Orthogonal fluorescent chemogenetic reporters for multicolor imaging. *Nat Chem Biol* **2021**, *17*(1), 30-38.

10. Lukinavicius, G.; Reymond, L.; Umezawa, K.; Sallin, O.; D'Este, E.; Gottfert, F.; Ta, H.; Hell, S. W.; Urano, Y.; Johnsson, K., Fluorogenic Probes for Multicolor Imaging in Living Cells. *J Am Chem Soc* **2016**, *138* (30), 9365-8.

11. Lavis, L. D.; Raines, R. T., Bright building blocks for chemical biology. *ACS Chem Biol* **2014**, *9* (4), 855-66.

12. Yamamoto, K.; Kamiya, M.; Urano, Y., Highly sensitive fluorescence imaging of cancer with avidin-protease probe conjugate. *Bioorg Med Chem Lett* **2019**, *29* (20), 126663.

13. Uno, S. N.; Kamiya, M.; Yoshihara, T.; Sugawara, K.; Okabe, K.; Tarhan, M. C.; Fujita, H.; Funatsu, T.; Okada, Y.; Tobita, S.; Urano, Y., A spontaneously blinking fluorophore based on intramolecular spirocyclization for live-cell super-resolution imaging. *Nat Chem* **2014**, *6* (8), 681-9.
14. Yasuteru Urano, M. S., Nobuyuki Kosaka, Mikako Ogawa, Makoto Mitsunaga, Daisuke Asanuma, Mako Kamiya, Matthew R. Young, Tetsuo Nagano, Peter L. Choyke, Hisataka Kobayashi, Rapid Cancer Detection by Topically Spraying a  $\gamma$ -Glutamyltranspeptidase-Activated Fluorescent Probe. *Science Translational Medicine* **2011**, *3* (110), 110ra119
15. Kenmoku, S.; Urano, Y.; Kojima, H.; Nagano, T., Development of a Highly Specific Rhodamine-Based Fluorescence Probe for Hypochlorous Acid and Its Application to Real-Time Imaging of Phagocytosis. *Journal of the American Chemical Society* **2007**, *129* (23), 7313-7318.
16. Koide, Y.; Urano, Y.; Hanaoka, K.; Terai, T.; Nagano, T., Development of an Si-Rhodamine-Based Far-Red to Near-Infrared Fluorescence Probe Selective for Hypochlorous Acid and Its Applications for Biological Imaging. *Journal of the American Chemical Society* **2011**, *133* (15), 5680-5682.

17. Sakabe, M.; Asanuma, D.; Kamiya, M.; Iwatate, R. J.; Hanaoka, K.; Terai, T.; Nagano, T.; Urano, Y., Rational Design of Highly Sensitive Fluorescence Probes for Protease and Glycosidase Based on Precisely Controlled Spirocyclization. *Journal of the American Chemical Society* **2013**, *135* (1), 409-414.
18. Asanuma, D.; Sakabe, M.; Kamiya, M.; Yamamoto, K.; Hiratake, J.; Ogawa, M.; Kosaka, N.; Choyke, P. L.; Nagano, T.; Kobayashi, H.; Urano, Y., Sensitive  $\beta$ -galactosidase-targeting fluorescence probe for visualizing small peritoneal metastatic tumours in vivo. *Nature Communications* **2015**, *6*, 6463.
19. Tachibana, R.; Kamiya, M.; Suzuki, S.; Morokuma, K.; Nanjo, A.; Urano, Y., Molecular design strategy of fluorogenic probes based on quantum chemical prediction of intramolecular spirocyclization. *Communications Chemistry* **2020**, *3* (1).
20. Mitchison, T. J.; Sawin, K. E.; Theriot, J. A.; Gee, K.; Mallavarapu, A., [4] Caged fluorescent probes. In *Methods in Enzymology*, Academic Press: 1998; Vol. 291, pp 63-78.
21. Puliti, D.; Warther, D.; Orange, C.; Specht, A.; Goeldner, M., Small

photoactivatable molecules for controlled fluorescence activation in living cells. *Bioorg Med Chem* **2011**, *19* (3), 1023-9.

22. Grimm, J. B.; Klein, T.; Kopek, B. G.; Shtengel, G.; Hess, H. F.; Sauer, M.; Lavis, L. D., Synthesis of a Far-Red Photoactivatable Silicon-Containing Rhodamine for Super-Resolution Microscopy. *Angew Chem Int Ed Engl* **2016**, *55* (5), 1723-7.

23. Grimm, J. B.; English, B. P.; Choi, H.; Muthusamy, A. K.; Mehl, B. P.; Dong, P.; Brown, T. A.; Lippincott-Schwartz, J.; Liu, Z.; Lionnet, T.; Lavis, L. D., Bright photoactivatable fluorophores for single-molecule imaging. *Nat Methods* **2016**, *13* (12), 985-988.

24. Frei, M. S.; Hoess, P.; Lampe, M.; Nijmeijer, B.; Kueblbeck, M.; Ellenberg, J.; Wadepohl, H.; Ries, J.; Pitsch, S.; Reymond, L.; Johnsson, K., Photoactivation of silicon rhodamines via a light-induced protonation. *Nature Communications* **2019**, *10* (1), 4580.

25. Zhao, Y.; Zheng, Q.; Dakin, K.; Xu, K.; Martinez, M. L.; Li, W. H., New caged coumarin fluorophores with extraordinary uncaging cross sections suitable for biological imaging applications. *J Am Chem Soc* **2004**, *126* (14), 4653-63.

26. Maurel, D.; Banala, S.; Laroche, T.; Johnsson, K., Photoactivatable and Photoconvertible Fluorescent Probes for Protein Labeling. *ACS Chemical Biology* **2010**, *5* (5), 507-516.
27. Hauke, S.; von Appen, A.; Quidwai, T.; Ries, J.; Wombacher, R., Specific protein labeling with caged fluorophores for dual-color imaging and super-resolution microscopy in living cells. *Chemical science* **2017**, *8* (1), 559-566.
28. Dakin, K.; Zhao, Y.; Li, W. H., LAMP, a new imaging assay of gap junctional communication unveils that Ca<sup>2+</sup> influx inhibits cell coupling. *Nat Methods* **2005**, *2* (1), 55-62.
29. Kobayashi, T.; Komatsu, T.; Kamiya, M.; Campos, C.; Gonzalez-Gaitan, M.; Terai, T.; Hanaoka, K.; Nagano, T.; Urano, Y., Highly activatable and environment-insensitive optical highlighters for selective spatiotemporal imaging of target proteins. *J Am Chem Soc* **2012**, *134* (27), 11153-60.
30. Likhotkin, I.; Lincoln, R.; Bossi, M. L.; Butkevich, A. N.; Hell, S. W., Photoactivatable Large Stokes Shift Fluorophores for Multicolor Nanoscopy. *J Am Chem Soc* **2023**, *145* (3), 1530-1534.

31. Kozłowski, D. J.; Murakami, T.; Ho, R. K.; Weinberg, E. S.,  
Regional cell movement and tissue patterning in the zebrafish embryo  
revealed by fate mapping with caged fluorescein. *Biochemistry and Cell  
Biology* **1997**, *75* (5), 551-562.
32. J.Kozłowski, K. R. G. S. W., Caged Q-rhodamine dextran: a new  
photoactivated fluorescent tracer. *Bioorganic & Medicinal Chemistry  
Letters* **2001**, *11* (16), 2181-2183.
33. Guo, Y. M.; Chen, S.; Shetty, P.; Zheng, G.; Lin, R.; Li, W. H.,  
Imaging dynamic cell-cell junctional coupling in vivo using Trojan-LAMP.  
*Nat Methods* **2008**, *5* (9), 835-41.
34. Dai, S.-Y.; Yang, D., A Visible and Near-Infrared Light Activatable  
Diazocoumarin Probe for Fluorogenic Protein Labeling in Living Cells.  
*Journal of the American Chemical Society* **2020**, *142* (40), 17156-17166.
35. Cauwel, M.; Guillou, C.; Renault, K.; Schapman, D.; Bénard, M.;  
Galas, L.; Cosette, P.; Renard, P.-Y.; Sabot, C., 3-Benzoylquinoxalinone as  
a photoaffinity labelling derivative with fluorogenic properties allowing  
reaction monitoring under “no-wash” conditions. *Chemical Communications*  
**2021**, *57* (32), 3893-3896.



36. Doura, T.; Kamiya, M.; Obata, F.; Yamaguchi, Y.; Hiyama, T. Y.; Matsuda, T.; Fukamizu, A.; Noda, M.; Miura, M.; Urano, Y., Detection of LacZ-Positive Cells in Living Tissue with Single-Cell Resolution. *Angew Chem Int Ed Engl* **2016**, *55* (33), 9620-4.
37. Obara, R.; Kamiya, M.; Tanaka, Y.; Abe, A.; Kojima, R.; Kawaguchi, T.; Sugawara, M.; Takahashi, A.; Noda, T.; Urano, Y., gamma-Glutamyltranspeptidase (GGT)-Activatable Fluorescence Probe for Durable Tumor Imaging. *Angew Chem Int Ed Engl* **2021**, *60* (4), 2125-2129.
38. Myers, J.; Widlanski, T., Mechanism-based inactivation of prostatic acid phosphatase. *Science* **1993**, *262* (5138), 1451-1453.
39. Lu, C.-P.; Ren, C.-T.; Wu, S.-H.; Chu, C.-Y.; Lo, L.-C., Development of an Activity-Based Probe for Steroid Sulfatases. *ChemBioChem* **2007**, *8* (18), 2187-2190.
40. Komatsu, T.; Kikuchi, K.; Takakusa, H.; Hanaoka, K.; Ueno, T.; Kamiya, M.; Urano, Y.; Nagano, T., Design and Synthesis of an Enzyme Activity-Based Labeling Molecule with Fluorescence Spectral Change. *Journal of the American Chemical Society* **2006**, *128* (50), 15946-15947.
41. Kwan, D. H.; Chen, H.-M.; Ratananikom, K.; Hancock, S. M.;

- Watanabe, Y.; Kongsaree, P. T.; Samuels, A. L.; Withers, S. G., Self-Immobilizing Fluorogenic Imaging Agents of Enzyme Activity. *Angewandte Chemie International Edition* **2011**, *50* (1), 300-303.
42. Haba, K.; Popkov, M.; Shamis, M.; Lerner, R. A.; Barbas, C. F.; Shabat, D., Single-Triggered Trimeric Prodrugs. *Angewandte Chemie International Edition* **2005**, *44* (5), 716-720.
43. Kashima, H.; Kamiya, M.; Obata, F.; Kojima, R.; Nakano, S.; Miura, M.; Urano, Y., Photoactivatable fluorophores for durable labelling of individual cells. *Chem Commun (Camb)* **2021**, *57* (47), 5802-5805.
44. Jack H. Kaplan, B. F., III, and Joseph F. Hoffman, Rapid Photolytic Release of Adenosine 5'-Triphosphate from a Protected Analogue: Utilization by the Na:K Pump of Human Red Blood Cell Ghosts. *Biochemistry* **1978**, *17* (10), 1929-1935.
45. Wilson, T. M. D. a. H. C., Chromophores for the Delivery of Bioactive Molecules with Two-Photon Excitation. *Neuromethods* **2011**, *55*, 57-92.
46. Kamiya, M.; Asanuma, D.; Kuranaga, E.; Takeishi, A.; Sakabe, M.; Miura, M.; Nagano, T.; Urano, Y., beta-Galactosidase fluorescence probe with improved cellular accumulation based on a spirocyclized rhodol

scaffold. *J Am Chem Soc* **2011**, *133* (33), 12960-3.

47. Butkevich, A. N.; Bossi, M. L.; Lukinavicius, G.; Hell, S. W., Triarylmethane Fluorophores Resistant to Oxidative Photobleaching. *J Am Chem Soc* **2019**, *141* (2), 981-989.

48. Hobro, A. J.; Smith, N. I., An evaluation of fixation methods: Spatial and compositional cellular changes observed by Raman imaging. *Vibrational Spectroscopy* **2017**, *91*, 31-45.

49. Judy L. Bolton a, S. B. T. b., John A. Thompson, Influence of quinone methide reactivity on the alkylation of thiol and amino groups in proteins: studies utilizing amino acid and peptide models. *Chemico-Biological Interactions* **1997**, *107*, 185-200.

50. Kwan, D. H.; Chen, H. M.; Ratananikom, K.; Hancock, S. M.; Watanabe, Y.; Kongsaree, P. T.; Samuels, A. L.; Withers, S. G., Self-immobilizing fluorogenic imaging agents of enzyme activity. *Angew Chem Int Ed Engl* **2011**, *50* (1), 300-3.

51. Liu, J.; Li, S.; Aslam, N. A.; Zheng, F.; Yang, B.; Cheng, R.; Wang, N.; Rozovsky, S.; Wang, P. G.; Wang, Q.; Wang, L., Genetically Encoding Photocaged Quinone Methide to Multitarget Protein Residues

Covalently in Vivo. *J Am Chem Soc* **2019**, *141* (24), 9458-9462.

52. Ueo, H.; Shinden, Y.; Tobo, T.; Gamachi, A.; Udo, M.; Komatsu, H.; Nambara, S.; Saito, T.; Ueda, M.; Hirata, H.; Sakimura, S.; Takano, Y.; Uchi, R.; Kurashige, J.; Akiyoshi, S.; Iguchi, T.; Eguchi, H.; Sugimachi, K.; Kubota, Y.; Kai, Y.; Shibuta, K.; Kijima, Y.; Yoshinaka, H.; Natsugoe, S.; Mori, M.; Maehara, Y.; Sakabe, M.; Kamiya, M.; Kakareka, J. W.; Pohida, T. J.; Choyke, P. L.; Kobayashi, H.; Ueo, H.; Urano, Y.; Mimori, K., Rapid intraoperative visualization of breast lesions with gamma-glutamyl hydroxymethyl rhodamine green. *Sci Rep* **2015**, *5*, 12080.

53. Shimane, T.; Aizawa, H.; Koike, T.; Kamiya, M.; Urano, Y.; Kurita, H., Oral cancer intraoperative detection by topically spraying a gamma-glutamyl transpeptidase-activated fluorescent probe. *Oral Oncol* **2016**, *54*, e16-8.

54. Mizushima, T.; Ohnishi, S.; Shimizu, Y.; Hatanaka, Y.; Hatanaka, K. C.; Hosono, H.; Kubota, Y.; Natsuizaka, M.; Kamiya, M.; Ono, S.; Homma, A.; Kato, M.; Sakamoto, N.; Urano, Y., Fluorescent imaging of superficial head and neck squamous cell carcinoma using a gamma-

glutamyltranspeptidase-activated targeting agent: a pilot study. *BMC*

*Cancer* **2016**, *16*, 411.

55. Miyata, Y.; Ishizawa, T.; Kamiya, M.; Yamashita, S.; Hasegawa, K.; Ushiku, A.; Shibahara, J.; Fukayama, M.; Urano, Y.; Kokudo, N.,

Intraoperative imaging of hepatic cancers using gamma-

glutamyltranspeptidase-specific fluorophore enabling real-time

identification and estimation of recurrence. *Sci Rep* **2017**, *7*(1), 3542.

56. Onoyama, H.; Kamiya, M.; Kuriki, Y.; Komatsu, T.; Abe, H.;

Tsuji, Y.; Yagi, K.; Yamagata, Y.; Aikou, S.; Nishida, M.; Mori, K.;

Yamashita, H.; Fujishiro, M.; Nomura, S.; Shimizu, N.; Fukayama, M.;

Koike, K.; Urano, Y.; Seto, Y., Rapid and sensitive detection of early

esophageal squamous cell carcinoma with fluorescence probe targeting

dipeptidylpeptidase IV. *Sci Rep* **2016**, *6*, 26399.

57. Ogasawara, A.; Kamiya, M.; Sakamoto, K.; Kuriki, Y.; Fujita, K.;

Komatsu, T.; Ueno, T.; Hanaoka, K.; Onoyama, H.; Abe, H.; Tsuji, Y.;

Fujishiro, M.; Koike, K.; Fukayama, M.; Seto, Y.; Urano, Y., Red

Fluorescence Probe Targeted to Dipeptidylpeptidase-IV for Highly Sensitive

Detection of Esophageal Cancer. *Bioconjug Chem* **2019**, *30* (4), 1055-1060.

58. Fujita, K.; Kamiya, M.; Yoshioka, T.; Ogasawara, A.; Hino, R.; Kojima, R.; Ueo, H.; Urano, Y., Rapid and Accurate Visualization of Breast Tumors with a Fluorescent Probe Targeting  $\alpha$ -Mannosidase 2C1. *ACS Cent Sci* **2020**, *6* (12), 2217-2227.
59. Sednev, M. V.; Wurm, C. A.; Belov, V. N.; Hell, S. W., Carborhodol: a new hybrid fluorophore obtained by combination of fluorescein and carbopyronine dye cores. *Bioconjug Chem* **2013**, *24* (4), 690-700.
60. Uno, S. N.; Kamiya, M.; Morozumi, A.; Urano, Y., A green-light-emitting, spontaneously blinking fluorophore based on intramolecular spirocyclization for dual-colour super-resolution imaging. *Chem Commun (Camb)* **2017**, *54* (1), 102-105.
61. Ito, H.; Kawamata, Y.; Kamiya, M.; Tsuda-Sakurai, K.; Tanaka, S.; Ueno, T.; Komatsu, T.; Hanaoka, K.; Okabe, S.; Miura, M.; Urano, Y., Red-Shifted Fluorogenic Substrate for Detection of lacZ-Positive Cells in Living Tissue with Single-Cell Resolution. *Angew Chem Int Ed Engl* **2018**, *57* (48), 15702-15706.
62. Bort, G.; Gallavardin, T.; Ogden, D.; Dalko, P. I., From one-photon to two-photon probes: "caged" compounds, actuators, and photoswitches.

*Angew Chem Int Ed Engl* **2013**, *52* (17), 4526-37.

63. Chiba, M.; Kamiya, M.; Tsuda-Sakurai, K.; Fujisawa, Y.;  
Kosakamoto, H.; Kojima, R.; Miura, M.; Urano, Y., Activatable  
Photosensitizer for Targeted Ablation of lacZ-Positive Cells with Single-Cell  
Resolution. *ACS Cent Sci* **2019**, *5* (10), 1676-1681.

64. Rivas, C.; Kamiya, M.; Urano, Y., A novel sialidase-activatable  
fluorescence probe with improved stability for the sensitive detection of  
sialidase. *Bioorg Med Chem Lett* **2020**, *30* (2), 126860.

## 謝辞

本研究を遂行するにあたり、多くのご支援とご指導を賜りました、東京大学 大学院医学系研究科 生体物理医学専攻 生体情報学分野 浦野 泰照 教授に深く感謝申し上げます。自由に研究できる最高の環境とその機会を頂けたこと、研究の方針に関する的確なご指摘を通して幅広い視点と本質を求める考え方を学ばせて頂きました。

研究活動において丁寧かつ多大なご指導を賜りました、東京工業大学 生命理工学院 神谷 真子 教授に心から深く御礼申し上げます。研究のいろはを改めて真摯にご教授頂いたこと、何事にも熱心に取り組む姿勢を自ら示して頂いたことなど、先生のもとでしか経験できなかった大変多くの学びがありました。研究生生活を総じてお力添えを頂き、大変お世話になりましたこと感謝申し上げます。

研究生生活において数多くのご助言を頂きました、東京大学 大学院医学系研究科 生体物理医学専攻 生体情報学分野 小嶋 良輔 准教授、藤田 恭平 助教、Sascha Keller 博士、河谷 稔 博士、小原 塁 博士に深く感謝致します。研究へのアドバイスはもちろんのこと、日頃の些細な相談にも乗って頂き、常に異なる観点から頂くご意見に公私ともに助けて頂きました。

また、同分野並びに薬学系研究科薬品代謝化学教室の教室員の皆様に深く感謝申し上げます。皆様と過ごした日々は常に自分にとって新鮮で貴重な時間でした。6年間の楽しい研究室生活をありがとうございました。

最後に、これまでの人生において生活を共にし、自由と元気を与えてくれた家族に深く感謝致します。

2023 年 1 月

生体物理医学専攻 生体情報学教室

鹿島 大幹